Burns & Trauma, 2024, 12, tkae009
https://doi.org/10.1093/burnst/tkae009
Research Article

OXFORD

Research Article

Immunomodulatory poly(L-lactic acid) nanofibrous membranes promote diabetic wound healing by inhibiting inflammation, oxidation and bacterial infection

Yan Wu[1,†], Jin Zhang[1,2,†], Anqi Lin[3,†], Tinglin Zhang[4], Yong Liu[5], Chunlei Zhang[5], Yongkui Yin[1], Ran Guo[6], Jie Gao[4,*], Yulin Li[3,*] and Yanhui Chu[1,*]

[1]Heilongjiang Key Laboratory of Tissue Damage and Repair, Mudanjiang Medical University, 3 Tongxiang Street, Aimin District, Mudanjiang 157011, China, [2]Clinical Laboratory, Zhejiang Medical & Health Group Quzhou Hospital, 62 Wenchang Road, Kecheng District, Quzhou 324004, China, [3]The Key Laboratory for Ultrafine Materials of Ministry of Education, State Key Laboratory of Bioreactor Engineering, Engineering Research Center for Biomedical Materials of Ministry of Education, School of Materials Science and Engineering, East China University of Science and Technology, 130 Meilong Road, Lingyun Street, Xuhui District, Shanghai 200237, China, [4]Changhai Clinical Research Unit, Shanghai Changhai Hospital, Naval Medical University, 168 Changhai Road, Yangpu District, Shanghai 200433, China, [5]Scientific Research Sharing Platform, Mudanjiang Medical University, 3 Tongxiang Street, Aimin District, Mudanjiang 157011, China and [6]Department of Physiology, Mudanjiang Medical University, 3 Tongxiang Street, Aimin District, Mudanjiang 157011, China

*Correspondence. Jie Gao, Email: jmsx2021@shu.edu.cn; Yulin Li, Email: yulinli@ecust.edu.cn; Yanhui Chu, Email: yanhui_chu@sina.com

[†]Yan Wu, Jin Zhang and Anqi Lin contributed equally to this work.

Received 11 April 2023; Revised 21 February 2024; Accepted 22 February 2024

Abstract

Background: Given the significant impact on human health, it is imperative to develop novel treatment approaches for diabetic wounds, which are prevalent and serious complications of diabetes. The diabetic wound microenvironment has a high level of reactive oxygen species (ROS) and an imbalance between proinflammatory and anti-inflammatory cells/factors, which hamper the healing of chronic wounds. This study aimed to develop poly(L-lactic acid) (PLLA) nanofibrous membranes incorporating curcumin and silver nanoparticles (AgNPs), defined as PLLA/C/Ag, for diabetic wound healing.

Methods: PLLA/C/Ag were fabricated via an air-jet spinning approach. The membranes underwent preparation and characterization through various techniques including Fourier-transform infrared spectroscopy, measurement of water contact angle, X-ray photoelectron spectroscopy, X-ray diffraction, scanning electron microscopy, assessment of *in vitro* release of curcumin and Ag^+, testing of mechanical strength, flexibility, water absorption and biodegradability. In addition, the antioxidant, antibacterial and anti-inflammatory properties of the membranes were evaluated *in vitro*, and the ability of the membranes to heal wounds was tested *in vivo* using diabetic mice.

Results: Loose hydrophilic nanofibrous membranes with uniform fibre sizes were prepared through air-jet spinning. The membranes enabled the efficient and sustained release of curcumin. More importantly, antibacterial AgNPs were successfully reduced *in situ* from $AgNO_3$. The incorporation

© The Author(s) 2024. Published by Oxford University Press.
This is an Open Access article distributed under the terms of the Creative Commons Attribution Non-Commercial License (https://creativecommons.org/licenses/by-nc/4.0/), which permits non-commercial re-use, distribution, and reproduction in any medium, provided the original work is properly cited. For commercial re-use, please contact journals.permissions@oup.com

Downloaded from academic.oup.com/burnstrauma/article/doi/10.1093/burnst/tkae009/7687763 by guest on 13 October 2026

of AgNPs endowed the membrane with superior antibacterial activity, and the bioactivities of curcumin and the AgNPs gave the membrane efficient ROS scavenging and immunomodulatory effects, which protected cells from oxidative damage and reduced inflammation. Further results from animal studies indicated that the PLLA/C/Ag membranes had the most efficient wound healing properties, which were achieved by stimulating angiogenesis and collagen deposition and inhibiting inflammation.

Conclusions: In this research, we successfully fabricated PLLA/C/Ag membranes that possess properties of antioxidants, antibacterial agents and anti-inflammatory agents, which can aid in the process of wound healing. Modulating wound inflammation, these new PLLA/C/Ag membranes serve as a novel dressing to enhance the healing of diabetic wounds.

Key words: Nanofibrous membrane, Poly(L-lactic acid), Curcumin, Silver nanoparticles, Autophagy, Wound healing, Diabetic wound, Inflammation, Oxidation, Infection, Bacterial

Highlights

- Tannic acid has multiple phenolic hydroxyl groups with highly potent reducing activity, which can induce the chemical reduction of $AgNO_3$ to form AgNPs *in situ*.
- Poly(L-lactic acid) nanofibrous membranes incorporated with curcumin and silver nanoparticles (AgNPs), defined as PLLA/C/Ag, were fabricated via an air-jet spinning approach.
- Curcumin and AgNP introduction can improve the immunomodulatory effects of PLLA membrane, so that it also has efficient ROS-scavenging ability and antibacterial activity compared with native PLLA film.
- The hybrid nanofibrous films can obviously promote the skin regeneration process.

Background

Diabetes is a common long-term metabolic condition. According to the latest article [1], the number of individuals diagnosed with diabetes worldwide was ~463 million in 2019, with a projected rise to 700 million by 2045. Chronic diabetic wounds, which are common but severe complications of diabetes, are characterized by long-term inflammation, delayed wound closure, severe infection and impaired angiogenesis [2,3]. Therefore, the development of novel therapeutic strategies with anti-inflammatory, antioxidant and antibacterial effects is necessary to accelerate the healing of diabetic wounds [4]. Traditional diabetic wound treatments include glycaemic control, wound debridement, topical or systematic antibiotic treatment and wound dressings [5,6]. However, wound dressings have traditionally served as only passive protective measures, have either limited or different success rates among patients and are not cost-effective. Bioactive substance-based therapies for diabetic wounds include those that use growth factors [7–9], protein formulations such as substance P [10], erythropoietin [11], insulin [12] and natural products. The delivery and bioavailability of these components at the wound site require an appropriate vehicle. As materials technology advances, active wound dressings that can efficiently deliver bioactive substances, such as films, foams and hydrogels, have been developed. Nevertheless, it is not feasible to efficiently transport bioactive compounds in a straightforward manner to the highest degree achievable. Consequently, dressings that imitate the extracellular matrix (ECM) and function as scaffolds and drug conveyors may offer improved management for diabetic wounds.

The Food and Drug Administration has approved poly(L-lactic acid) (PLLA) due to its exceptional biocompatibility and mechanical properties which make it a perfect substrate for wound healing dressings [13]. PLLA nanofibrous membranes fabricated *in situ* by air-jet spinning (a convenient and effective nanofibre-spinning technique) [14,15] have a high specific surface area and unique simulated ECM structure that can promote cell adhesion and skin regeneration [16], making them an ideal scaffold to promote wound healing. We previously used air-jet spinning to prepare PLLA nanofibrous membranes that promoted diabetic wound healing by regulating the reactive oxygen species (ROS) in the immune microenvironment [17]. Recently, many researchers have incorporated various bioactive substances, such as growth factors, stem cells, other compounds from nature and synthetic materials, into nanofibrous membranes [18–20]. Because diabetic wounds are multifactorial and complicated, specific interventions for a single symptom are not sufficient to remarkably promote wound healing. For example, because infection is not the only cause of prolonged inflammation, only protecting the wound site from microbial invasion might not trigger healing [21]. Similarly, although persistent inflammation impedes diabetic wound healing, inhibiting inflammation alone is not sufficient to promote healing. The most effective way to promote healing of diabetic wounds is by combining various therapeutic methods that possess anti-inflammatory, antioxidant and antibacterial properties. Therefore, we speculated that introducing additional bioactive substances into PLLA nanofibrous membranes may improve diabetic wound healing.

Downloaded from academic.oup.com/burnstrauma/article/doi/10.1093/burnst/tkae009/7687763 by guest on 13 October 2026

Curcumin, the active component of the rhizome of *Curcuma longa* L., contributes to the promotion of wound healing due to its antioxidant and anti-inflammatory activities and ability by facilitating wound contraction, formation of granulation tissue, tissue remodeling and deposition of collagen [22–25]. Nevertheless, the utilization of curcumin is greatly restricted due to its inadequate solubility in water, limited ability to be absorbed orally and unstable chemical nature [26]. It has been reported that several components and techniques can enhance the bioavailability of curcumin. Delivering curcumin via various drug delivery systems increases its efficiency and bioavailability, thereby increasing its potential applications [26]. Notably, topical application can directly target diseased areas at an appropriate drug concentration, thereby preventing unpredictable absorption into other organs and tissues. Therefore, this route represents the most promising strategy for treating diabetic wounds [27]. Nanofibrous membranes, known for their softness and large surface area relative to volume, are highly effective dressings for the application of topical drugs and delivery of therapeutic agents to enhance the healing of diabetic wounds [28]. Several studies have reported that curcumin-loaded nanofibrous membranes can sustainably release curcumin, thereby increasing its stability, bioavailability and therapeutic efficacy [29,30].

Delayed wound healing is significantly influenced by bacterial infections [31]. The effectiveness of systemic antibiotics in treating skin infections is limited and the prolonged use of antibiotics leads to drug resistance, dysbacteriosis and other motor complications [32]. Therefore, at present, local medical therapy is preferred for treating skin infections; however, the therapeutic effects of conventional local therapy do not last long, and their prolonged use leads to bacterial resistance [33]. Silver nanoparticles (AgNPs) are well-known metal NPs that have been employed for medicinal purposes owing to their potent antimicrobial properties [34]. According to recent research, AgNPs have been found to have antibacterial properties against various pathogenic microorganisms and drug-resistant pathogens [35]. Considering the antioxidant, anti-inflammatory and antibacterial effects of curcumin and AgNPs, their codelivery by and sustained release through PLLA nanofibrous membranes may help to synergistically accelerate diabetic wound healing.

The immune response to tissue damage is critical for regulating the quality and duration of diabetic wound healing [36]. In response to injury, inflammatory (M1 phenotype) macrophages transform into the anti-inflammatory M2 phenotype. M2 macrophages with immunosuppressive and anti-inflammatory properties contribute to inflammation control and ECM remodelling during wound healing. As a result, the shift of macrophages towards the M2 phenotype has become an attractive strategy for promoting healing in individuals with diabetes [36]. Autophagy is an evolutionarily conserved process that catabolizes intracellular components to recycle nutrients to produce energy and regenerate organelles through lysosomes. The relationship between autophagy and macrophage polarization is complex. Autophagy can interfere with the polarization of macrophages. Autophagy dysfunction in macrophages leads to polarization towards the M1 phenotype, thereby exacerbating the inflammatory response [37]. Conversely, the activation of autophagy prompts macrophages to polarize towards the M2 phenotype, resulting in a reduction in the inflammatory response and an acceleration in healing. Consequently, inducing autophagy by using autophagy activators leads to macrophage polarization towards the M2 phenotype, consequently decreasing the inflammatory response in the wound and enhancing the rate of healing [38]. Autophagy inhibitors cause macrophages to polarize towards the M1 phenotype, leading to more severe tissue damage. Consistent with the findings of most studies, we previously reported that inhibiting autophagy with gold NPs can promote M1 polarization [39]. Hence, we hypothesized that stimulating autophagy could be a viable approach to enhance the polarization of macrophages towards the M2 phenotype. Considering the fact that curcumin and AgNPs are widely recognized as triggers of autophagy [40,41], our hypothesis is that by utilizing AgNPs and curcumin to induce autophagy, macrophages can transition from a proinflammatory M1 state to an anti-inflammatory M2 state. This transformation would lead to successful management of inflammation and remodeling of the ECM, ultimately facilitating the healing of diabetic wounds. In this study, we used air-jet spinning to prepare PLLA nanofibrous membranes incorporating AgNPs and curcumin (PLLA/C/Ag membranes). The multiple properties and functions of the membranes will be confirmed, including their biocompatibility and antibacterial, antioxidant and anti-inflammatory activities.

Methods

Materials

L-Lactide was purchased from Jinan Daigang Biomaterial Co., Ltd (Jinan, China). Shanghai Lingfeng Chemical Reagent Co., Ltd (Shanghai, China) supplied the dichloromethane and glutaraldehyde. Sinopharm Chemical Reagent Co., Ltd (Shanghai, China) provided tannic acid and silver nitrate ($AgNO_3$). Beijing Solarbio Science & Technology Co., Ltd (Beijing, China) supplied curcumin and streptozotocin. Beyotime Biotechnology Co., Ltd (Shanghai, China) provided the following substances: hydrogen peroxide (H_2O_2), 3-(4,5-dimethylthiazol-2-yl)-2,5-diphenyltetrazolium bromide (MTT), a kit for measuring ROS, an AdPlus-mCherry-green fluorescent protein (GFP)-LC3B assay kit, a kit for double-staining with calcein acetoxymethyl ester (calcein-AM) and propidium iodide (PI), a kit for measuring superoxide dismutase (SOD), and 4,6-diamino-2-phenyl indole (DAPI), phosphate-buffered saline (PBS), bicinchoninic acid assay (BCA) protein quantification Kit. The mouse embryonic fibroblast line NIH-3 T3 and macrophage-like cell line RAW 264.7 were obtained from Shanghai EK-Bioscience Biotechnology Co., Ltd (Shanghai, China).

Downloaded from academic.oup.com/burnstrauma/article/doi/10.1093/burnst/tkae009/7687763 by guest on 13 October 2026

Dulbecco's modified Eagle's medium (DMEM), 0.25% trypsin and fetal bovine serum were purchased from Gibco Life Technologies (Carlsbad, CA, USA). Omega Bio-Tek, Inc. (Doraville, GA, USA) was the source of the RNA extraction kit. Roche Pharmaceutical Ltd (Basel, Switzerland) provided a high-capacity cDNA reverse transcription kit and SYBR Green Master Mix. *Staphylococcus aureus* (JZ113) and *Escherichia coli* (JZ112) were acquired from Hunan Fenghui Biotechnology Co., Ltd (Wuhan, China). Methicillin-resistant Staphylococcus aureus (MRSA) were acquired from ning bo testobio Co., Ltd (Ningbo, China). C57BL/6 mice, aged between 8 and 10 weeks, were acquired from Beijing Huafukang Biology Technology Co., Ltd (Beijing, China). The antibodies against cluster of differentiation 206 (CD206) and cluster of differentiation 86 (CD86) were obtained from Affinity Biosciences Co., Ltd (Jiangsu, China). Cell Signaling Technology, Inc. (Beverly, MA, USA) provided the α-smooth muscle actin (α-SMA) and microtubule-associated proteins light chain 3 (LC3) A/B antibodies, while the anti-Platelet endothelial cell adhesion molecule-1 (CD31) antibody was obtained from Abcam (Cambridge, UK). Shanghai Jingkang Bioengineering Co., Ltd (Shanghai, China) provided the interleukin 6 (IL-6) and tumor necrosis factor α (TNF-α) enzyme-linked immunosorbent assay (ELISA) kits.

Preparation and characterization of multifunctional nanofibrous membranes

Synthesis of PLLA In our previous study [17], PLLA was created through the ring-opening polymerization of L-lactide with $Sn(Oct)_2$ as the catalyst, at 140°C for 6 h. Pure PLLA was obtained by purifying the raw material through dissolution and precipitation using methylene chloride and ethanol. The resulting product was then dried in a vacuum oven at 40°C for 48 h.

Fabrication of PLLA and PLLA/C nanofibrous membranes by airbrushing The PLLA and PLLA/C nanofibrous membranes were fabricated via the air-jet spinning approach as described previously [17]. In short, PLLA and PLLA/C were dissolved in methylene chloride while being stirred magnetically for 4 h. The mixture was then sprayed using a commercial airbrush (HD-130, Syou Tools, China) with a nozzle diameter of 0.5 mm. The spraying was done at a pressure of 0.2 MPa, with the collector placed 20 cm away from the nozzle for all samples. All samples were dried in a vacuum oven for 48 h to obtain PLLA or PLLA/C nanofibrous membranes.

Fabrication of AgNP-loaded PLLA nanofibrous membranes PLLA nanofibrous membranes loaded with AgNPs were prepared via the *in situ* chemical reduction of $AgNO_3$ using tannic acid as the reducing agent. Briefly, PLLA nanofibrous membranes were subjected to ammonia plasma treatment for 1 min at a power of 50 W to introduce amino groups onto the surface of the membranes as active sites. Following activation, the membranes were submerged in glutaraldehyde (7.5%) and left to incubate at 37°C for 2 h. Subsequently, tannic acid was introduced at a concentration of 13 mg/ml. The nanofibrous membranes containing tannic acid were rinsed thrice with deionized water after 6 h. Subsequently, they were submerged in a solution of $AgNO_3$ (1 mg/ml) and placed on a shaker at 37°C for 6 h in the absence of light. Thereafter, the membranes were rinsed with deionized water and vacuum-dried at 40°C for 2 days to obtain PLLA nanofibrous membranes loaded with AgNPs. The following designations are used: PLLA nanofibrous membranes, PLLA/C nanofibrous membranes (PLLA nanofibrous membranes loaded with curcumin), PLLA/Ag nanofibrous membranes (PLLA nanofibrous membranes loaded with AgNPs) and PLLA/C/Ag nanofibrous membranes (PLLA nanofibrous membranes loaded with curcumin and AgNPs).

Fourier-transform infrared spectroscopy Fourier-transform infrared (FTIR) spectroscopy (Nicolet 5700, Thermo, Waltham, MA, USA) was used to analyse the chemical composition of the PLLA nanofibrous membranes. The examination was conducted in the wavelength range 4000–400 cm^{-1}, with 32 scans at a resolution of 4 cm^{-1}. The FTIR spectra were analyzed using the OPUS Viewer software (version 6.5) from Bruker (Ettlingen, Germany).

Water contact angle measurements The water affinity of the PLLA nanofibrous membranes was assessed by employing a contact angle meter (JC2000D2, Zhongchen Instruments, Shanghai, China). Briefly, the prepared membranes were cut into 1 × 1 cm squares. One drop of water (3 μl) was applied from the needle tip to the membrane surface, and a high-resolution camera was used to capture images of the droplet on the surface of the membrane. Subsequently, the water droplet images were analysed, and the contact angles were estimated.

X-Ray photoelectron spectroscopy analysis For qualitative and quantitative analysis of nitrogen (N) on the membranes, the PLLA nanofibrous membranes underwent narrow scanning using X-ray photoelectron spectroscopy (XPS) (ESCALAB 250Xi, Thermo Fisher, MA, USA) before and after treatment with ammonia plasma. All binding energies were referenced to the neutral carbon peak (C1s) at 285 eV.

X-Ray diffraction analysis The PLLA nanofibrous membranes' crystalline formations were examined by employing an X-ray polycrystalline diffractometer (D8 Advance, Bruker, Ettlingen, Germany) equipped with a Cu Kα source (λ = 0.15418 nm) and powered by a 40 kV potential. After the membranes were prepared, they were cut into a circular shape measuring 10 mm in diameter. Subsequently, the samples were mounted on a glass slide and spectra were obtained. The X-ray angle (2θ) was adjusted from 10 to 80°, utilizing a resolution of 0.02° and scanning at a rate of 3° per min. Using Jade 7, a specific X-ray diffraction (XRD) spectrum analysis software by Materials Data, Inc. (Livermore, CA,

Downloaded from academic.oup.com/burnstrauma/article/doi/10.1093/burnst/tkae009/7687763 by guest on 13 October 2026

USA), the XRD spectra were analyzed to estimate the degree of crystallinity (Xc) for each sample.

Morphological characterization FESEM (Hitachi S-4800, Tokyo, Japan) was used to characterize the morphologies of the PLLA nanofibrous membranes. Prior to obtaining images, the membranes' surfaces were treated with gold (Au) for about 60 s using a sputter-coating machine (Quorum SC7620, ABD, East Sussex, UK) with an accelerating voltage of 15 kV. ImageJ software (National Institutes of Health, MD, USA) was utilized to analyse the mean fibre diameter and distribution of sizes. Energy-dispersive X-ray spectroscopy (EDS) was used to analyse the distribution of elements on the surface of the membrane. The analysis was conducted using Quanta 200 FEG, FEI Co. (Hillsboro, OR, USA).

Drug loading and *in vitro* release of curcumin from the nanofibrous membranes The incorporation of curcumin into the PLLA nanofibrous membranes was assessed as described below. In short, a solution of PLLA nanofibrous membranes (10 mg) was prepared by dissolving them in methylene chloride (10 ml) at 25°C. The absorbance of each sample was then determined at a wavelength of 421 nm using a microplate reader (Spectra Max M2, Molecular Devices, Silicon Valley, CA, USA). Thereafter, the concentration of curcumin was determined using a standard curve of curcumin dissolved in methylene chloride.

The *in vitro* release of curcumin from the PLLA nanofibrous membranes was examined as described below. In summary, 6 mg of nanofibrous membranes was placed into a solution of 10 ml of PBS that contained 0.5% Tween-20. The membranes were then incubated on a shaker at 37°C for 120 h (using a THZ-100B shaker from Yiheng Scientific Instrument Co., Ltd, located in Shanghai, China). At regular intervals, 1 ml of PBS was removed and the absorbance of the solution was measured using a microplate reader at a wavelength of 421 nm. Thereafter, the concentration of curcumin was determined using a standard curve of curcumin dissolved in PBS containing 0.5% Tween-20.

Grafting rate of nanosilver particles and *in vitro* release of Ag^+ from the nanofibrous membranes The grafting rate of the nanosilver particles was determined as follows. First, a 500 mg/ml $AgNO_3$ solution was prepared in which to soak the PLLA/C/N membrane. After 6 h, the remaining immersion solution was collected, the Ag^+ concentration in the solution was meausured by an inductively coupled plasma emission spectrometer (NexION 2000-(A-10), USA) and the grafting rate of the nanosilver particles was determined by calculating the difference in concentration.

The *in vitro* release of Ag^+ from the PLLA/C/Ag nanofibre membranes was detected as follows. In short, a nanofibre membrane weighing 10 mg was placed in 10 ml of PBS solution with 0.5% Tween-20 and incubated on a shaker (THZ-100B, Yiheng Technology Instrument Co., Ltd, Shanghai, China) at 37°C for 1, 3, 5 and 7 days. At regular intervals, 1 ml of PBS was taken out and diluted by a factor of 10 to determine the concentration of Ag^+ using inductively coupled plasma spectrometry.

Mechanical strength test The PLLA/C/Ag nanomembrane was cut into a dumbbell-shaped spline (gauge distance of 25 mm) with a cutter and tested on a universal testing machine (SANS CMT 2503, USA) according to the national standard GB/T 1040–2006 with a tensile rate of 10 mm/min, a test temperature of 25°C and three parallel group tests.

Flexibility and water absorption testing The flexibility test is briefly described as follows. PLLA/C/Ag was attached to a piece of pig skin, and the pig skin was arbitrarily twisted to observe the state of the nanofilm as the pig skin changed.

To measure the water absorption by the PLLA/C/Ag nanofibre membranes, initially 10 mg of the nanofibre membranes were soaked in 10 ml of PBS solution containing 0.5% Tween-20 for incubation on a shaker (THZ-100B, Yiheng Technology Instrument Co., Ltd, Shanghai, China) at 37°C for 1, 3, 5 and 7 days. At regular intervals, the membrane was taken out, its surface moisture was absorbed and the membrane was weighed.

$$\text{Water absorption } (\%) = \frac{W_{\text{Wet film}}}{W_{\text{Dry film}}} * 100\%$$

Biodegradability of the nanofibrous membranes For the evaluation of the degradability of the PLLA nanofibrous membranes, a 10 mg piece of the membrane was placed in 10 ml of PBS and incubated on a shaker (HZ-9610KBTHZ-100B, Yiheng Scientific Instrument Co., Ltd, Shanghai, China) at a steady temperature of 37°C. Samples of PBS were collected at specific time points, and the pH was measured at each time point to evaluate the degradability of the membranes.

Biological evaluations

Assessing the biocompatibility of the nanofibrous membranes made from PLLA MTT assays and staining with calcein-AM and PI were used to assess the biocompatibility of the nanofibrous membranes made from PLLA. To conduct the MTT assays, aseptic PLLA nanofibrous membranes measuring 6 mm in diameter were immersed in 1 ml of DMEM at 37°C for 24 h. PLLA nanofibrous membranes were removed, and the the culture medium (extracted medium) is collected. A total of 5000 3 T3 fibroblasts were seeded in a 96-well plate and incubated for 24 h. Subsequently, they were exposed to the collected medium and cultured for a further 24 h at 37°C in the presence of 5% CO_2. Afterwards, the wells were loaded with 100 μl of MTT solution at a concentration of 5 mg/ml and the cells were then incubated for another 4 h. The absorbance of the wells at 490 nm was measured using microplate readers and the relative cell count was determined. To perform live/dead fluorescence staining, NIH-3 T3 cells were cultivated in 6-well plates with cell climbing slices and

Downloaded from academic.oup.com/burnstrauma/article/doi/10.1093/burnst/tkae009/7687763 by guest on 13 October 2026

incubated for 12 h. The medium (2 ml) obtained through the aforementioned process was then gathered and introduced into every culture plate. After 24 h, calcein-AM and PI were applied to the cells for 15 min at 25°C after removing the medium. Confocal microscopy (Olympus FV1000, Olympus, Tokyo, Japan) was utilized to observe and capture images of the cells.

Wound healing assay PLLAs nanofibrous membranes, which were sterile and had a size of 6 mm in diameter, were subjected to incubation with 1 ml of DMEM at 37°C for 24 h. The extracted medium from this process was utilized for the *in vitro* wound healing assay, as mentioned in [42]. NIH-3T3 cells with exponential growth were placed in 6-well trays (5×10^5 cells per well) and incubated for 24 h. Once the cells achieved 90% confluency, a scratch was made using a 100 μl pipette tip to evaluate cell migration. After adding the extracted medium to the cells, cell culture was continued for 12–24 h. The cells incubated without the membrane samples served as the blank control group. Photographs were taken under an optical microscope (Nikon, FHEIPSE Ti, Tokyo, Japan) to observe cell migration at various time intervals. The relative area of cell migration was calculated by determining the cell-free gap area using ImageJ. This calculation was done using the equation: relative area of cell migration $(\%) = (WA_0 - WA_t)/WA_0 \times 100$. Here, WA_0 represents the initial wound area and WA_t represents the wound area at time t.

***In vitro* antibacterial activity** The antibacterial efficacy of PLLA nanofibrous membranes was assessed against *E. coli*, *S. aureus* and *MRSA* strains (both gram-negative and gram-positive) through the utilization of the plate-counting method, zone of inhibition test and evaluation of bacterial concentration. To perform the plate-counting technique, *E. coli*, *S. aureus* and *MRSA* were diluted with Luria–Bertani (LB) medium to achieve a working concentration of 1×10^7 colony-forming units (CFU)/ml. Afterwards, 4 ml of bacterial cultures and three pieces of PLLA nanofibrous membrane measuring 8 mm in diameter were introduced into 5 ml Eppendorf tubes for coexistence for 24 h at a steady temperature of 37°C [220 revolutions per minute (rpm)]. Then, ~100 μl of each sample was removed from the Eppendorf tube and gently spread onto an agar plate, which was incubated in an inverted position for 24 h. Subsequently, cell colonies on the surface were observed using captured images. To conduct the zone of inhibition experiment, 50 μl of bacterial culture (1×10^7 CFU per ml) were added to 5 ml of LB medium and incubated overnight at 37°C with constant shaking at 220 rpm. Overnight cultures of bacterial strains were evenly coated on LB agar plates. Nanofibrous membranes 8 mm in diameter that had been irradiated by UV overnight were placed on the LB agar plate coated with bacteria. A constant temperature incubator was used for 24 h of culture at 37°C. The diameter of the bacteriostatic ring was measured and recorded. In order to determine the amount of bacteria present, 4 ml of bacterial cultures (1×10^7 CFU/ml) and three nanofibrous membrane slices measuring 8 mm in diameter were placed into 5-ml Eppendorf tubes. These tubes were then incubated at a constant temperature of 37°C for 24 h at a speed of 220 rpm. The increase in the bacterial strains was observed every 3 h by assessing the optical density at 600 nm (OD_{600}) using a microplate reader.

Antioxidant assays

Cytoprotection in the presence of H_2O_2 Antioxidant assay was performed by incubating 6 mm sterile PLLA nanofibrous membranes with 1 ml of DMEM at 37°C for 24 h, and the extracted medium was collected as the medium for analysis. NIH-3T3 cells were seeded in 96-well plates at a density of 5×10^3 cells per well and cultured with a medium containing 600 μM H_2O_2, either with or without the addition of the extracted medium, for 24 h. Following that, cell viability assays were conducted using the MTT technique outlined in the Biological evaluations section above.

Intracellular ROS elimination assay As described previously, the measurement of 2′-7′-dichlorofluorescein diacetate (DCFH-DA) oxidation was used to evaluate intracellular levels of ROS [43]. The brightness of DCF is directly linked to the amount of ROS present within the cell. In summary, aseptic PLLA nanofibrous membranes measuring 6 mm in diameter were immersed in 1 ml of cell culture medium and kept at 37°C for 24 h. The extracted medium obtained after incubation was utilized for the antioxidant assay. NIH-3T3 cells were grown in 96-well black microporous plates for 24 h, with a cell density of 5×10^3 cells per well. The culture medium was removed, and 50 μl of the extracted medium and 50 μl of H_2O_2 were added to the cells for 24 h of treatment. Following that, the cells were placed in PBS with 10 μM DCFH-DA and incubated for 30 min. Finally, the levels of ROS were measured using a microplate reader at an excitation wavelength of 485 nm and an emission wavelength of 525 nm. Additionally, the cellular fluorescence signal was visualized using a confocal microscope. In short, NIH-3T3 cells were grown in 6-well dishes with 3×10^5 cells per well and treated with culture medium containing 600 μM H_2O_2 with or without the extracted medium for 24 h. Then, the medium was discarded and the cells were exposed to 10 μM DCFH-DA solution at 37°C for 30 min in the absence of light. The cells were washed and the nuclei were counterstained with Hoechst (5 μg/ml) for 10 min. Fluorescence was analysed via confocal microscopy.

SOD assay The level of SOD, which catalyses the transformation of superoxide anions into H_2O_2 and O_2, was determined using a colorimetric SOD assay kit. In short, aseptic PLLA nanofibre filters measuring 6 mm in diameter were immersed in 1 ml of DMEM at 37°C for 24 h. The extracted medium obtained from this process was used to measure the SOD concentration. The extracted medium was used to treat NIH-3T3 cells, which were then digested and washed twice with cold PBS. To extract protein, the cells were

Downloaded from academic.oup.com/burnstrauma/article/doi/10.1093/burnst/tkae009/7687763 by guest on 13 October 2026

disrupted in radioimmunoprecipitation assay solution for 15 min, followed by centrifugation of the lysates at 12,000 g and 4°C for 5 min. A BCA protein assay kit was used to quantitate the protein in the supernatants (Beyotime Biotechnology, Shanghai, China). Finally, based on the manufacturer's instructions, SOD levels were determined using commercially available kits.

Western blotting Cells were homogenized in radioimmunoprecipitation assay buffer for protein extraction. After undergoing sodium dodecyl sulfate–polyacrylamide gel electrophoresis, the proteins that were isolated were then transferred onto nitrocellulose membranes. Following a 2-h incubation at 25°C in the presence of 5% BSA, the membranes were subsequently subjected to overnight incubation at 4°C with the primary antibodies, including anti-CD86 (1 : 1000), anti-CD206 (1 : 1000), anti-LC3 (1 : 1000), anti-P62 (1 : 1000) and anti-glyceraldehyde-3-phosphate dehydrogenase (1 : 1000). Afterwards, the protein bands were observed using enhanced chemiluminescence reagent and the analysis of their density was conducted using ImageJ software.

Analysis of the effect of the nanofibrous membranes on macrophage polarization Nanofibrous membranes made of sterile PLLA, measuring 6 mm in diameter, were subjected to incubation with 1 ml of cell culture medium at 7°C for 24 h. The extracted medium obtained from this process was utilized for quantitative reverse transcription polymerase chain reaction (qRT-PCR). Analysis of inflammation-related mRNA expression [CD206, IL-6, arginase 1 (Arg-1), CD86, TNF-α and transforming growth factor β (TGF-β)] in RAW 264.7 macrophages was performed via qRT–PCR. The macrophages were placed in 6-well tissue culture dishes with a density of 5×10^5 cells per well for 12 h. Afterwards, they were exposed to lipopolysaccharide (LPS) (1 μg/ml) with or without the presence of the extracted medium. Following a 24-h incubation period, the manufacturer's instructions were followed to extract total RNA using TRIzol reagent, which was then reverse transcribed using a reverse transcription kit. Following that, PCR was performed on an ABI Step One device (Applied Biosystems, Los Angeles, CA, USA) using SYBR Green Master Mix. For every reaction, β-actin served as the internal control. The sequences of the primers used in the experiment are listed in Table 1.

Transfection of mRFP-GFP-LC3 adenovirus AdPlus-mCherry-GFP-LC3B adenovirus was used to infect RAW 264.7 cells (3×10^5) in 6-well plates for 12 h at a multiplicity of infection of 10. After transfection, the macrophages were incubated with the extracted medium before coculture for 24 h. A confocal microscope was used to observe and calculate the numbers of autophagosomes (green$^+$ red$^+$) and autolysosomes (green$^-$ red$^+$). After dividing the number of puncta by the number of cells, the ratio of fluorescent puncta was used to analyse autophagic flux.

Table 1. Sequences of the primers used for qRT–PCR

Name of primer	Primer sequence
M-CD86-F	ACGGAGTCAATGAAGATTTCCT
M-CD86-R	GATTCGGCTTCTTGTGACATAC
TNF-α-F	CCCTCACACTCAGATCATCTTCT
TNF-α-R	GCTACGACGTGGGCTACAG
M-IL-6-F	CTCCCAACAGACCTGTCTATAC
M-IL-6-R	CCATTGCACAACTCTTTTCTCA
CD206-F	CCTATGAAAATTGGGCTTACGG
CD206-R	CTGACAAATCCAGTTGTTGAGG
TGF-β-F	CCCTCACACTCAGATCATCTTCT
TGF-β-R	GCTACGACGTGGGCTACAG
Arg-1-F	TTGGGTGGATGCTCACACTG
Arg-1-R	TTGCCCATGCAGATTCCC
β-Actin-F	CTTTGCAGCTCCTTCGTTGC
β-Actin-R	ACGATGGAGGGGAATACAGC

In vivo studies Male C57BL/6 mice were acquired from Beijing Huafukang Biological Technology Co., Ltd (Beijing, China) for *in vivo* experiments. The Ethics Committee on Animals of Mudanjiang Medical University ensured that all experiments conducted on animals adhered to their guidelines. The mice were housed in pathogen-free conditions, with temperature-controlled rooms (20–24°C) and 50–60% relative humidity, following a 12-h light/dark cycle. Every mouse was provided with unlimited water and food during the entire experiment and was euthanized by inhaling CO_2. Every possible attempt was made to reduce the distress of the mice.

In vivo antibacterial activity The antibacterial effectiveness of the PLLA nanofibrous membranes in living organisms was examined in C57BL/6 mice, following the previously described method [4]. Briefly, all C57BL/6 mice (weighing 23–25 g and aged 10–12 weeks) were divided into five groups (n = 3) as follows: (1) control, (2) PLLA, (3) PLLA/Ag, (4) PLLA/C and (5) PLLA/C/Ag. Mice were anaesthetized with isoflurane and kept warm with a heating pad during surgery. The backs of the mice were shaved to expose the back skin and disinfected with 1% iodophor solution. Every mouse's dorsum was incised with two 8 mm round wounds symmetrically spaced. Sterile gauze (for the control group) and PLLA, PLLA/Ag, PLLA/C and PLLA/C/Ag nanofibrous membranes with a diameter of 8 mm were preseeded with an inoculum consisting of 10^7 CFU *S. aureus* and air-dried for 15 min. Thereafter, the gauze or nanofibrous membranes were subcutaneously implanted into the incisions, and the incisions were sutured. Three days after implantation, the mice were euthanized via CO_2 inhalation. Finally, the gauze or nanofibrous membranes were removed, and bacterial growth was observed and quantified using the plate-counting method.

***In vivo* wound healing assay** To induce diabetes similar to type 1, male C57BL/6 mice aged 8 and 10 weeks (weighing 20–23 g) were administered streptozotocin (100 mg/kg)

Downloaded from academic.oup.com/burnstrauma/article/doi/10.1093/burnst/tkae009/7687763 by guest on 13 October 2026

intraperitoneally for 2 days after fasting overnight, following the method described in [44]. After 2 weeks, the glucose levels in the blood were measured using a blood glucose monitor. Diabetic mice were exclusively those with a blood glucose concentration >16.7 mM, and subsequently, full-thickness cutaneous wounds were induced in these mice. A total of 45 diabetic mice were used for subsequent experiments. Two identical injuries, measuring 6 mm in diameter, were created on the posterior side of every mouse. The mice were divided into six groups in a random manner, which were named PLLA, PLLA/C, PLLA/Ag, PLLA/C/Ag, control and Tegaderm film. The diameter of all implanted membranes was 6 mm. The control group was treated with sterile gauze. All treated wounds were reinforced with parafilm tape to prevent detachment of the gauze or nanofibrous membranes. Tests on animals were carried out in a room that was free from specific pathogens. Using a digital camera, the wounds were photographed on days 0, 7 and 14 to observe the healing process on a macroscopic level. The rate of wound healing was evaluated using the following equation: wound healing rate $= (W_0 - W_t)/W_0$, where W_0 and W_t represent the wound area on day 0 and time t, respectively.

Histological and immunohistochemical analyses and western blotting To evaluate wound healing, staining was performed using haematoxylin and eosin (H&E), Masson's trichrome and picrosirius red as described previously [17]. Briefly, a portion of the skin from the wound site of a sacrificed mouse was taken and fixed in 4% paraformaldehyde. The samples were sequentially dipped in xylene and a mixture of xylene and ethanol, then encased in paraffin and sliced into 5-μm-thick slides with a tissue slicer (Leica RM2265, Biosystems, Wetzlar, Germany). After H&E, Masson and picrosirius red staining, tissue regeneration was examined with an optical microscope and a nanopolarized microscope (MF43-N, Guangzhou Microshot Technology Co., Ltd, Guangzhou, China). Alternatively, the skin samples were immersed in tissue freezing medium, frozen in dry ice–propanol, cut into 6-μm-thick sections and incubated with appropriate primary antibodies (anti-α-SMA, anti-CD31, anti-CD206, anti-CD86 and anti-LC3) at 4°C overnight. On the next day, the tissue samples were exposed to secondary antibodies (AffiniPure goat anti-rabbit IgG [H + L]) conjugated with Alexa Fluor® 550 for 2 h at ambient temperature.

Subsequently, DAPI was applied to the tissue sections for 5 min and antifluorescence quenching sealing tablets were used to mount the tissue sections. Protein localization in the cells was visualized using a laser scanning confocal microscope, and the density of fluorescence was quantified using ImageJ software. In order to examine macrophages at the site of the wound, the wound samples were sliced into small fragments and promptly immersed in a lysis solution containing 0.2% w/v of collagenase IV and 0.1% w/v of DNase I. During digestion, the samples were shaken at 90 rpm and 37°C for 60 min and vortexed every 20 min. The suspension was filtered using a 150-m filter and then suspended in red blood cell lysis buffer (Beyotime Biotechnology, China), followed by incubation on ice for 10 min. Thereafter, the expression of LC3 and P62 was analysed via western blotting as described above.

ELISAs ELISAs were used to evaluate inflammatory protein expression after nanofibrous membrane treatment. Tissue samples were excised for protein isolation. Following homogenization of the tissue, the BCA assay was used to determine the overall protein concentration. The expression of proteins related to inflammation (IL-6 and TNF-α) was assessed using ELISA kits.

Statistical analysis

The mean ± SD is given for all experimental data after analysis using GraphPad Prism Software (GraphPad Software, Inc., La Jolla, CA, USA). Student's t test was utilized to conduct comparisons between two groups. To compare multiple groups, we utilized one-way analysis of variance [45,46]. In cases where the data exhibited homogeneity of variance, the LSD test was utilized. Alternatively, Tamhane's T2 test was employed when the data did not meet the homogeneity of variance assumption. Significant differences were determined based on $p < 0.05$ ($^{*}p < 0.05$; $^{**}p < 0.01$; $^{***}p < 0.001$).

Results

Production and analysis of the PLLA nanofibrous membranes

In this study, air-jet spinning was used to fabricate PLLA nanofibrous membranes (Figure 1a). Curcumin was efficiently encapsulated in the membranes with a drug loading of 10.8%. As expected, the resulting PLLA/C membranes were bright yellow, indicating the successful incorporation of curcumin (Figure 1b). PLLA/C/Ag membranes (nanofibrous membranes encapsulating both curcumin and AgNPs) were prepared via the *in situ* chemical reduction of $AgNO_3$ using tannic acid as a reducing agent.

The presence of the encapsulated materials in the nanofibrous membranes was confirmed, and the functional groups were characterized using FTIR spectroscopy. Additionally, FTIR was utilized to distinguish the potential chemical alterations between phases [47]. Figure 1c shows the FTIR spectra of the nanofibrous membranes PLLA, PLLA/N, PLLA/C and PLLA/C/N, obtained within the wavelength range 4000–400 cm^{-1}. The nanofibrous membranes displayed two absorption peaks at 1749 and 1084 cm^{-1}, indicating the tensile vibrations of C=O and C–O in PLLA, respectively. In order to investigate the impact of ammonia plasma treatment on the initiation of membrane wettability, a comparison was made between the water contact angles of PLLA membranes with and without plasma treatment. As shown in Figure 1d, after plasma treatment, the contact angle of the PLLA membranes decreased from 109.3 ± 4.5 to 65.5 ± 3.2°, while the contact angle of the PLLA/C membranes decreased from 129.3 ± 5.3 to 79.4 ± 4.0°. This indicates a reduction in the

Downloaded from academic.oup.com/burnstrauma/article/doi/10.1093/burnst/tkae009/7687763 by guest on 13 October 2026

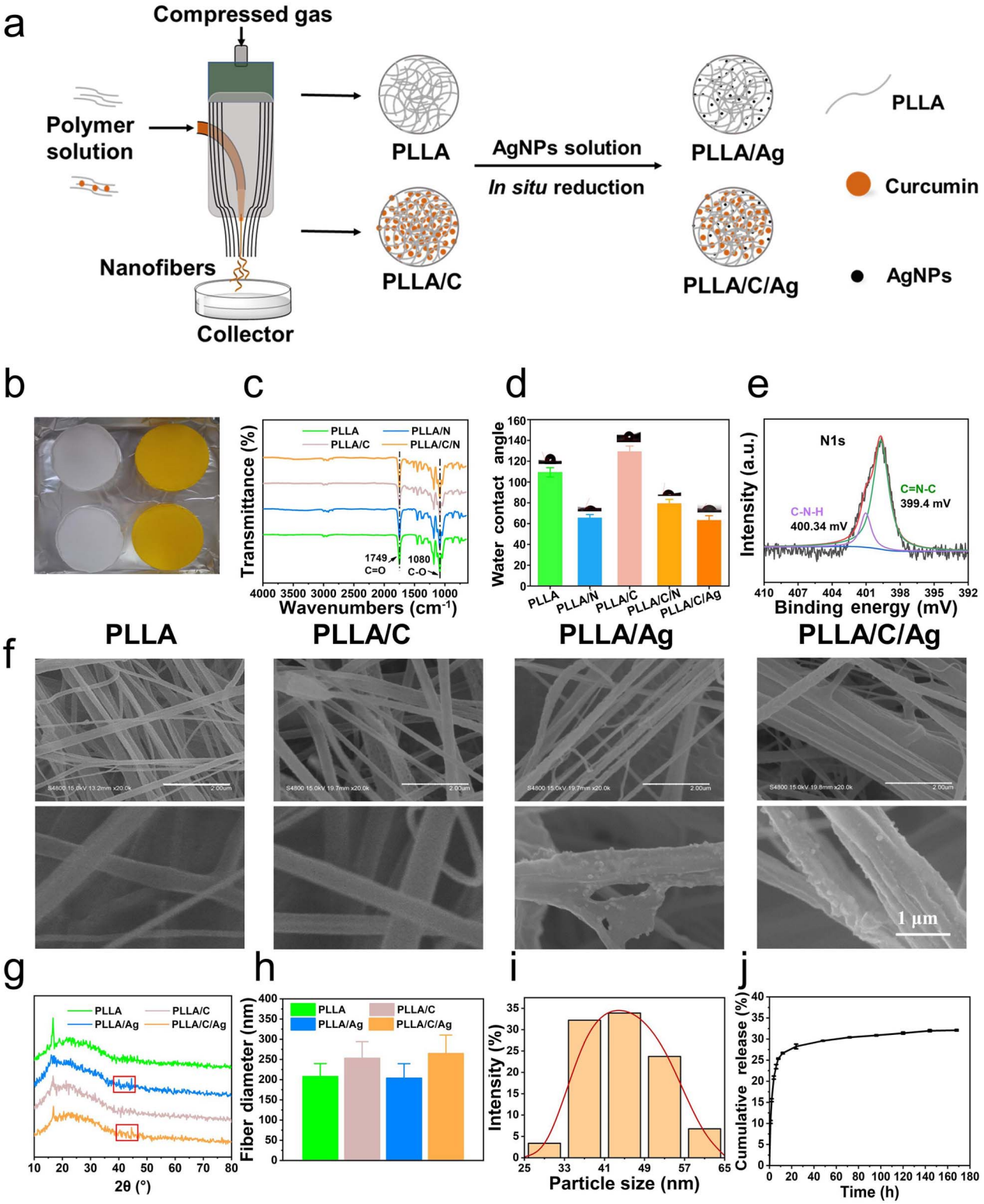

Figure 1. Development and physicochemical properties of PLLA nanofibrous membranes. (**a**) Schematic diagram of the development of PLLA nanofibrous membranes via air-jet spinning technology and *in situ* chemical reduction of $AgNO_3$. (**b**) Images of PLLA (left) and PLLA/C (right) nanofibrous membranes. (**c**) FTIR spectra and (**d**) water contact angles of PLLA nanofibrous membranes. (**e**) XPS spectra of PLLA/N nanofibrous membranes. (**f**) Morphology of PLLA nanofibrous membranes examined via SEM (upper scale bar: 2 μm; lower scale bar: 1 μm). (**g**) XRD patterns of PLLA nanofibrous membranes. (**h**) Average diameter of PLLA nanofibrous membranes. (**i**) Size distribution of AgNPs estimated from SEM images shown in (f). (**j**) Cumulative release of curcumin from PLLA/C nanofibrous membranes. Data are expressed as the mean ± SD (n = 3). *PLLA* poly(L-lactic acid), *PLLA/C* poly(L-lactic acid)/curcumin, *PLLA/N* poly(L-lactic acid)/nitrogen, *PLLA/Ag* poly(L-lactic acid)/silver nanoparticles, *PLLA/C/Ag* poly(L-lactic acid)/curcumin/silver nanoparticles, *AgNPs* silver nanoparticles, *XPS* X-ray photoelectron spectroscopy, *SEM* scanning electron microscope, *XRD* X-ray diffraction, *FTIR* Fourier-transform infrared spectrometry, *SD* standard deviation

Downloaded from academic.oup.com/burnstrauma/article/doi/10.1093/burnst/tkae009/7687763 by guest on 13 October 2026

contact angles of the PLLA and PLLA/C membranes of 40.1 and 38.6% respectively. We also conducted a contact angle test on the PLLA/C/Ag membranes. The findings indicated that the contact angle of the PLLA/C/Ag film, which had undergone grafting with AgNPs, measured $63.2 \pm 4.4°$. Furthermore, XPS was used to verify the presence and types of hydrophilic groups. As shown in Figure 1e, on the surface of the PLLA/N nanofibrous membrane, C–N–H and C=N–C groups, with a nitrogen content of 2.97% were found. Scanning electron microscopy (SEM) was utilized to examine the morphologies and structures of the PLLA membranes. ImageJ was used to calculate the diameter and size distribution of >100 randomly chosen nanofibres from the SEM images in the membrane. As shown in Figure 1f, h, the nanofibres of all membranes were distributed uniformly with a diameter of 150–350 nm, and the incorporation of curcumin appeared to slightly increase the diameter of the nanofibres.

XRD analysis was used to characterize the crystal structure of the PLLA membranes (Figure 1g). The PLLA and PLLA/C membrane samples did not show any diffraction peaks, whereas the PLLA/Ag and PLLA/C/Ag membranes had a diffraction peak at 44.52°, which belongs to the (200) crystallographic plane of the Ag face-centred cubic crystal plane structure [48]. Furthermore, SEM analysis validated the immobilization and homogeneous distribution of AgNPs on the PLLA/Ag and PLLA/C/Ag membranes. As calculated from the SEM images, the AgNPs had an average particle size of 44.5 ± 7.8 nm, with a narrow particle size distribution (30–60 nm) (Figure 1i). EDS was used to analyse the arrangement of components on the PLLA membrane surface. Both nitrogen and silver were detected on the membrane surface, which is consistent with the above-mentioned results (Figure S1, see online supplementary material). Additionally, the pH of the PBS solution in which the nanofibrous membranes were immersed decreased slightly from 7.4 to 7.1, indicating that the membranes have good biodegradability and can continue to degrade during drug release and wound healing without producing an excess of acidic products, which is beneficial for maintaining the stability of the wound environment (Figure S2a, see online supplementary material).

As shown in the release curve in Figure 1j, curcumin showed a burst release of 25% in the initial stage (10 h). After the first burst release, curcumin showed sustained and moderate release, with a cumulative release rate of >30% on day 7 of incubation. Because the bactericidal activity and cytotoxicity of AgNPs are dose dependent, we determined the loading and release of AgNPs. The results show that the grafting rate of the nanosilver particles was small, and most of the Ag^+ was removed by washing with deionized water. Furthermore, after 1, 3, 5 and 7 days of degradation, the spinning film released 0.0295 ± 0.00212, 0.1025 ± 0.00212, 0.113 ± 0.0099 mg/l and 0.1595 ± 0.07 mg/l of Ag^+, respectively. This gradual increase in the released quantity exhibited a specific antibacterial impact (Figure S2b, c). The PLLA/C/Ag membrane displayed advantageous mechanical characteristics, including a tensile strength of 7.081 MPa, an elongation at fracture of 18.848% and an elastic modulus of 72.125 MPa. Although the membrane was relatively brittle and less robust, it provided flexibility and the ability to bend and fold, which can be adjusted accordingly based on the conformation of the affected area (Figure S2d, e). Additionally, over 1, 3, 5 and 7 days, the PLLA/C/Ag membrane displayed water absorption rates of 112 ± 2.8, 155 ± 32.5, 229 ± 130.1 and 137 ± 38.9%, respectively (Figure S2f).

Biological evaluations

Biocompatibility of the nanofibrous membranes When nanofibrous membranes are applied to a wound, they come into close contact with the cells involved in healing. Therefore, for their successful application as wound dressings, it is essential that membranes are biocompatible. In this study, cell viability, migration and morphology were assessed by using live/dead staining, wound healing assays and MTT cell viability assays (Figure 2). First, NIH-3T3 cells were treated with PLLA nanofibrous membranes and stained with calcein-AM and PI (for live/dead staining) to assess the biocompatibility of the membranes. Living cells are indicated by green staining, whereas dead cells are indicated by red staining. As shown in Figure 2a, almost no red staining was observed, indicating that all of the fabricated membranes had low toxicity. Furthermore, the wound healing assay showed that NIH-3T3 cells treated with PLLA/C and PLLA/C/Ag membranes had markedly increased migration abilities at 12 and 24 h (Figure 2b, c). There was no notable disparity in cell migration between the PLLA and PLLA/Ag groups, and the membranes did not enhance cell migration compared to the control at any time point. The MTT assay showed that after 24 h in the presence of all membranes, the survival rates of different types of cells were >90%, suggesting the good biocompatibility of the nanofibrous membranes (Figure 2d). After being subcutaneously implanted into C57BL/6 mice, the *in vivo* biocompatibility of the nanofibrous membranes was also examined. After 2 weeks of implantation, there were no observed pathological alterations in the hearts, livers, spleens, lungs or kidneys of the mice (Figure S3, see online supplementary material). No notable variances were detected in the blood biochemical parameters (Figure S4, see online supplementary material). These results suggest that the PLLA/C/Ag membranes have good biocompatibility and low cytotoxicity and can support the survival and proliferation of skin cells.

Nanofibrous membranes made of PLLA exhibit antibacterial properties Nanofibrous membranes made of PLLA were tested to quantitatively determine their antibacterial activity. Gram-negative and gram-positive bacteria were respectively assessed for their antibacterial activity against the PLLA membrane using *E. coli* and *S. aureus* as model strains. Analysing bacterial growth curves at different time points offers insight into the antibacterial properties of PLLA

Downloaded from academic.oup.com/burnstrauma/article/doi/10.1093/burnst/tkae009/7687763 by guest on 13 October 2026

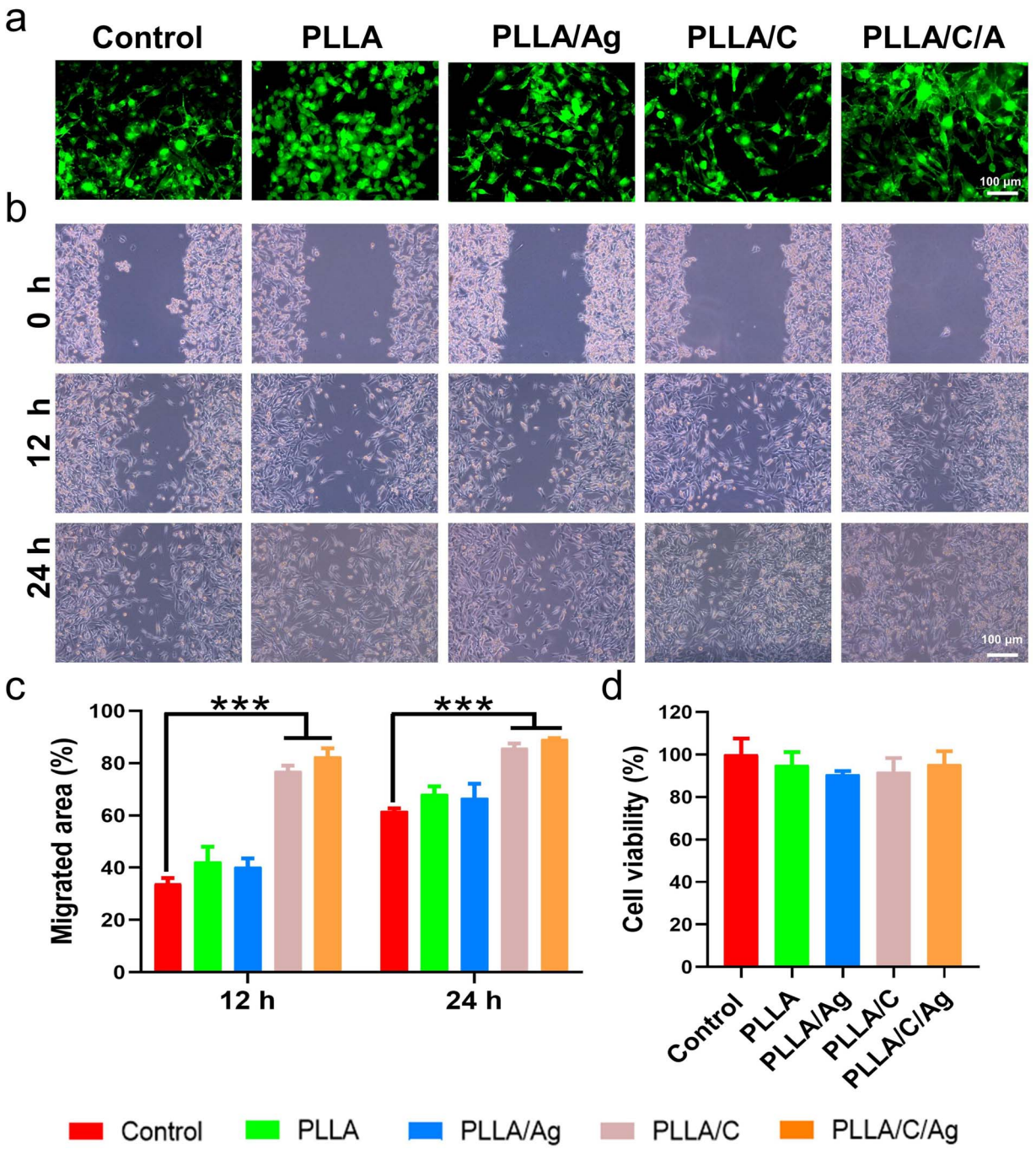

Figure 2. Biocompatibility of PLLA nanofibrous membranes. (**a**) Representative images of live/dead staining of NIH-3T3 cells with calcein-AM and PI after treatment with PLLA nanofibrous membranes for 24 h (scale bar: 100 μm). (**b**) Representative images of the wound healing assay of NIH-3T3 cells treated with PLLA nanofibrous membranes for 12 and 24 h (scale bar: 100 μm). (**c**) Quantitative analysis of cell migration evaluated via wound healing assay. (**d**) Viability of NIH-3T3 cells treated with PLLA nanofibrous membranes for 24 h. Data are expressed as the mean ± SD (n = 6) (***$p < 0.001$). *PLLA* poly(L-lactic acid), *PLLA/C* poly(L-lactic acid)/curcumin, *PLLA/Ag* poly(L-lactic acid)/silver nanoparticles, *PLLA/C/Ag* poly(L-lactic acid)/curcumin/silver nanoparticles, *calcein-AM* calcein acetoxymethyl ester, *PI* propidium iodide, *NIH* National Institutes of Health, *SD* standard deviation

nanofibrous membranes. As shown in Figure 3a, the antibacterial activities of the PLLA and PLLA/C membranes were negligible, whereas the PLLA/Ag and PLLA/C/Ag membranes remarkably inhibited bacterial growth. At 24 h, the absorbance (OD_{600}) value was significantly lower in the PLLA/Ag and PLLA/C/Ag groups than in the PLLA and control groups (Figure 3b). Additionally, the antimicrobial effects of the PLLA nanofibrous membranes were assessed through a cloning assay conducted on plates (Figure 3h). The antibacterial activity results, which were quantified, are displayed in Figure 3d. In the PLLA/Ag and PLLA/C/Ag groups, the survival rates of *E. coli* were 2.5 and 2.3%,

Downloaded from academic.oup.com/burnstrauma/article/doi/10.1093/burnst/tkae009/7687763 by guest on 13 October 2026

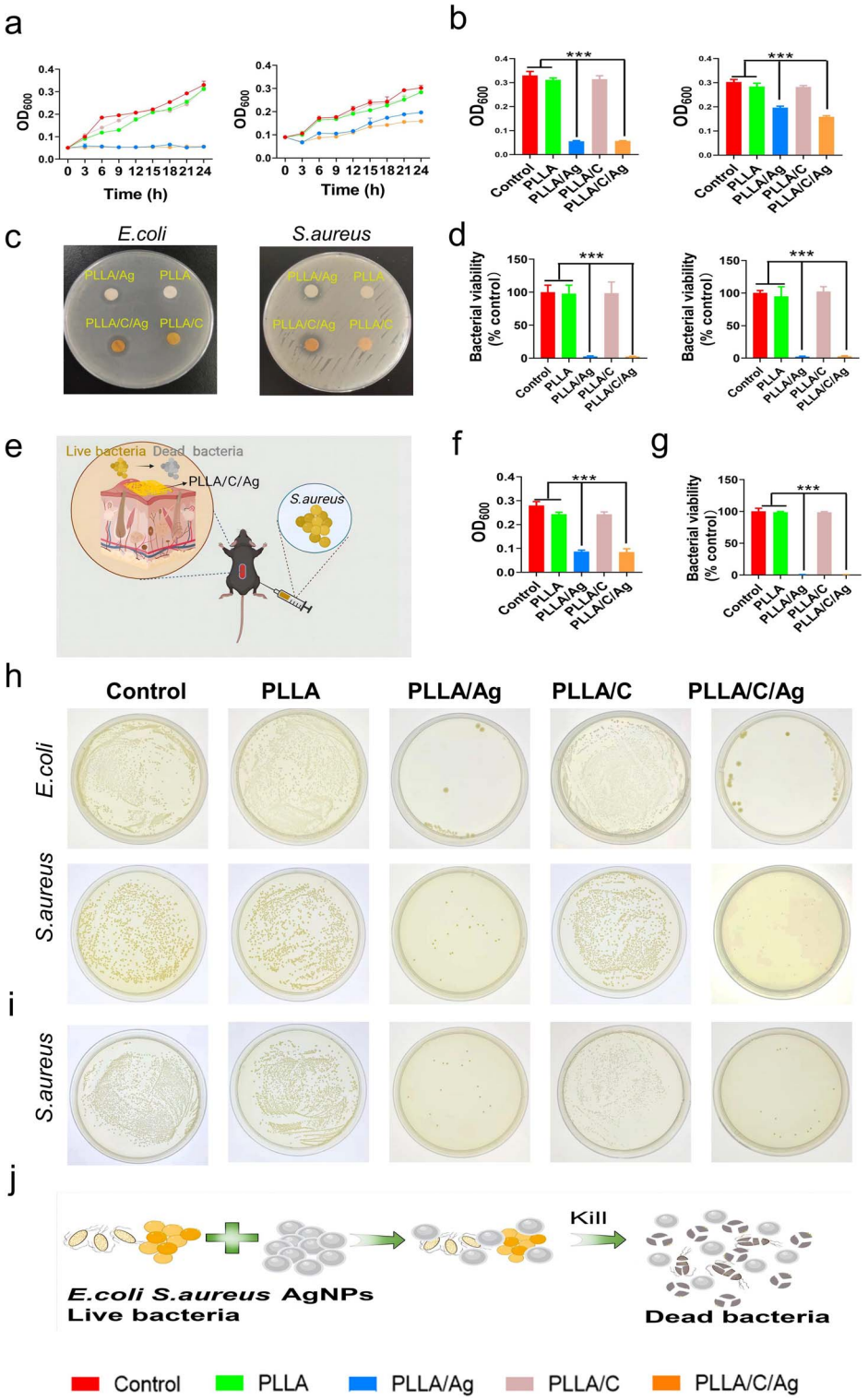

Figure 3. Antibacterial activity of PLLA nanofibrous membranes. (**a**) Bacterial growth curve based on the absorbance (OD_{600}) of samples treated with PLLA nanofibrous membranes. (**b**) Bacterial growth indicated by the absorbance (OD_{600}) value at 24 h. (**c**) The zone of inhibition for *E. coli* and *S. aureus* cultured with PLLA/Ag and PLLA/C/Ag membranes on agar plates. (**d**) *In vitro* antibacterial activity against *S. aureus and E. coli* quantified via a plate-based bacterial cloning assay. (**e**) Schematic illustration of *in vivo* antibacterial activity in a mouse model of diabetic wounds infected with *S. aureus*. (Image created with BioRender.com). (**f**) *In vivo* bacterial growth indicated by the absorbance (OD_{600}) value at 24 h. (**g**) *In vivo* antibacterial activity against *S. aureus* quantified via a plate-based bacterial cloning assay. Data are expressed as the mean ± SD (n = 3) ($^{***}p < 0.001$). (**h**) *In vitro* plate-based bacterial cloning assay after the culture of *E. coli* and *S. aureus* with PLLA nanofibrous membranes for 12 h. (**i**) *In vivo* plate-based bacterial cloning assay after the 12 h culture of *S. aureus* is plated from the mouse model of diabetic wounds infected with *S. aureus*. (**j**) Antibacterial mechanism of AgNPs. *PLLA* poly(L-lactic acid), *PLLA/C* poly(L-lactic acid)/curcumin, *PLLA/Ag* poly(L-lactic acid)/silver nanoparticles, *PLLA/C/Ag* poly(L-lactic acid)/curcumin/silver nanoparticles, *OD* optical density, *E. coli Escherichia coli*, *S. aureus Staphylococcus aureus*, *AgNPs* silver nanoparticles, *SD* standard deviation

Downloaded from academic.oup.com/burnstrauma/article/doi/10.1093/burnst/tkae009/7687763 by guest on 13 October 2026

respectively, and those of *S. aureus* were 2.1 and 2.6%, respectively. However, the antibacterial activity was minimal in the PLLA and PLLA/C groups. In the PLLA/Ag and PLLA/C/Ag groups, the zones of inhibition for *E. coli* and *S. aureus* were consistently larger compared to the PLLA and PLLA/C groups, as shown in Figure 3c.

The *in vivo* antibacterial efficacy of the PLLA nanofibrous membranes was evaluated using a mouse model of *S. aureus*-infected wounds, considering the aforementioned findings. The related scheme is shown in Figure 3e. *Staphylococcus aureus* was used as a model bacterium because it is responsible for the majority of skin infections [49]. An 8 mm long incision was created in the dorsum of each mouse and sutured after implantation of the nanofibrous membrane. After 3 days of culture, the wounds treated with gauze had evident festering with serious inflammation and suppuration, whereas the wounds treated with the PLLA/Ag or PLLA/C/Ag membranes had less suppuration. The implanted PLLA membranes were removed and the attached bacteria were collected. The antibacterial activity was substantially higher in the PLLA/Ag and PLLA/C/Ag groups than in the other groups, as determined by evaluating bacterial concentration (Figure 3f). Additionally, the attached bacteria were coated on agar plates and cultured for 24 h. Once again, as shown in data from the plate bacterial cloning assay (Figure 3i), the quantified trend in antibacterial activity was in line with the results in Figure 3f. The survival rates of the bacteria in the PLLA/Ag and PLLA/C/Ag groups were 0.86 and 0.68%, respectively. However, the antibacterial activity was minimal in the PLLA and PLLA/C groups (Figure 3g). In this study, we used AgNPs synthesized *in situ* to prevent bacterial infection in diabetic wounds. Figure 3j depicts the utilization of *E. coli* and *S. aureus*, both gram-negative and gram-positive bacteria, as representative microorganisms to investigate the *in vitro* antibacterial efficacy of diverse nanofibrous membranes. Similarly, many studies have reported the effectiveness of AgNPs against multidrug-resistant bacterial strains, such as *MRSA* [50]. Both the PLLA/Ag and PLLA/C/Ag membranes exhibited similar results and showed a certain effect against *MRSA* (Figure S6, see online supplementary material).

***In vitro* antioxidant assay** To assess the antioxidant activity of the nanofibrous membranes, cell models of oxidative stress were constructed by treating NIH-3T3 cells with various concentrations of H_2O_2 (Figure S5, see online supplementary material). As anticipated, the viability of cells declined in a manner that was dependent on the dosage and reached ~50% when exposed to 600 μM H_2O_2. Therefore, 600 μM H_2O_2 was selected as the optimal concentration to stimulate oxidative stress in cells.

In the presence of oxidative stress, the protective properties of the PLLA nanofibrous membranes were investigated. As anticipated, the viability of cells decreased considerably to 63% following treatment with H_2O_2. Additionally, PLLA did not attenuate the H_2O_2-induced decrease in cell viability. However, the addition of PLLA/Ag, PLLA/A/C and PLLA/C/Ag membranes remarkably improved cell viability at the same H_2O_2 concentration (Figure 4a). In order to investigate the impact of cytoprotection on the decrease in oxidative stress caused by ROS scavenging through PLLA nanofibrous membranes, the levels of intracellular ROS were assessed by employing the fluorescent probe DCFH-DA (Figure 4b, c). After its uptake by cells, DCFH-DA is deacetylated by cellular esterases to generate DCFH. Intracellular ROS oxidizes DCFH, which is unable to pass through the cell membrane, into fluorescent DCF [51]. The amount of intracellular ROS is directly correlated to the resulting fluorescence intensity of DCF. Upon treatment with H_2O_2, a high fluorescence signal was observed within the cell, which corresponded to the increased content of ROS in the cells. The fluorescence signal was not affected by the PLLA and PLLA/Ag membranes, but it significantly decreased when the PLLA/C and PLLA/C/Ag membranes were present, indicating that the PLLA nanofibrous membranes containing curcumin have effective abilities to scavenge ROS. Additionally, the relative intracellular fluorescence intensity was quantified using a microplate reader and the results were consistent with those obtained by fluorescence imaging (Figure 4d). SOD activity was evaluated with the SOD assay kit. In the presence of H_2O_2, SOD levels experienced a significant decrease; however, they showed a notable increase upon the addition of extracts from the PLLA/C and PLLA/C/Ag membranes (Figure 4e).

The nanofibrous membranes promoted macrophage polarization towards the M2 phenotype Macrophages, which are crucial inflammatory cells, play a significant role in regulating skin inflammation during the pathogenesis of diabetic wound healing [52]. Hence, an analysis was conducted on the impact of PLLA nanofibrous membranes on macrophages' immunomodulatory properties. To assess the *in vitro* anti-inflammatory characteristics of the PLLA nanofibrous membranes, the polarization of macrophages was examined using western blotting and qRT–PCR. LPS treatment stimulated the polarization of macrophages towards the M1 phenotype. Following the application of PLLA/Ag, PLLA/A/C and PLLA/C/Ag membranes, the levels of inflammatory cytokines in macrophages, including CD86, IL-6 and TNF-α, were significantly reduced, while the levels of anti-inflammatory cytokines, such as CD206, TGF-β and ARG1, were noticeably elevated (Figure 5a–f). Additional proof was the increase in CD86, a marker for M1 macrophages, and the decrease in CD206, a marker for M2 macrophages (Figure 5g and h). After treatment with the PLLA/Ag, PLLA/A/C and PLLA/C/Ag membranes, the expression of CD86 was significantly decreased ($p < 0.05$), whereas that of CD206 was significantly increased ($p < 0.05$). Similar results were observed for the expression of tissue inflammatory proteins, as detected via ELISA (Figure S7, see online supplementary material). These results suggest that treatment with the PLLA/Ag, PLLA/A/C and PLLA/C/Ag membranes

Downloaded from academic.oup.com/burnstrauma/article/doi/10.1093/burnst/tkae009/7687763 by guest on 13 October 2026

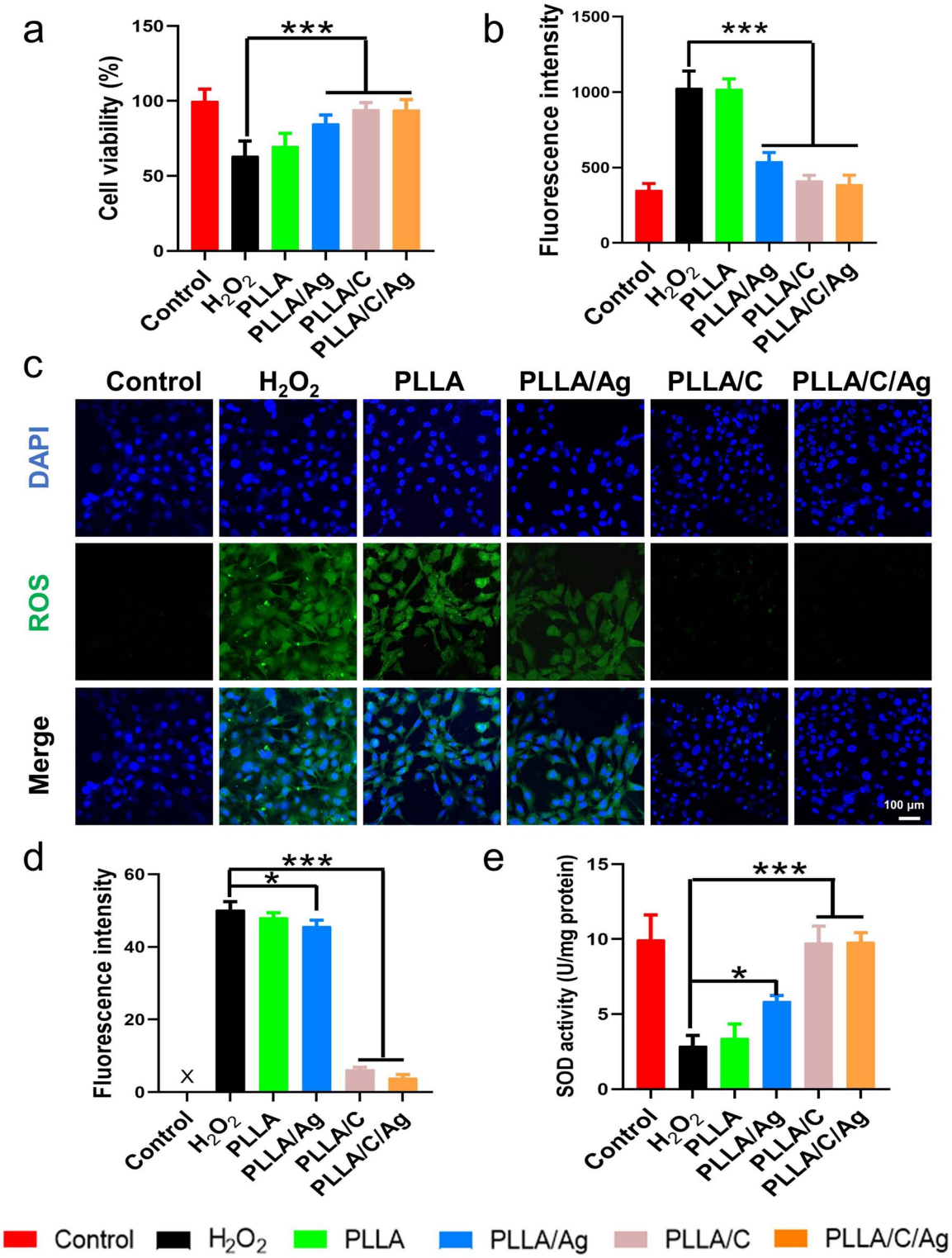

Figure 4. *In vitro* antioxidant assay. (**a**) Cytoprotective effects of PLLA nanofibrous membranes in the presence of oxidative stress (treatment with 600-μM H_2O_2). (**b**) Quantitative analysis of the fluorescence intensity of ROS. Data are expressed as the mean ± SD. (**c**) ROS-scavenging ability of PLLA nanofibrous membranes was examined using DCFH-DA as a fluorescent probe (scale bar: 100 μm). (**d**) Fluorescence intensity of ROS was quantified using a microplate reader. (**e**) SOD activity of H_2O_2-stimulated NIH-3 T3 cells. Data are expressed as the mean ± SD (n = 3) (* $p < 0.05$; *** $p < 0.001$). *PLLA* poly(L-lactic acid), PLLA/C poly(L-lactic acid)/curcumin, *PLLA/Ag* poly(L-lactic acid)/silver nanoparticles, *PLLA/C/Ag* poly(L-lactic acid)/curcumin/silver nanoparticles, *H_2O_2* hydrogen peroxide, *DAPI* 4′,6-diamidino-2-phenylindole, *ROS* reactive oxygen species, *SOD* superoxide dismutase, *DCFH-DA* 2′-7′-dichlorofluorescein diacetate, *NIH* National Institutes of Health, *SD* standard deviation

Downloaded from academic.oup.com/burnstrauma/article/doi/10.1093/burnst/tkae009/7687763 by guest on 13 October 2026

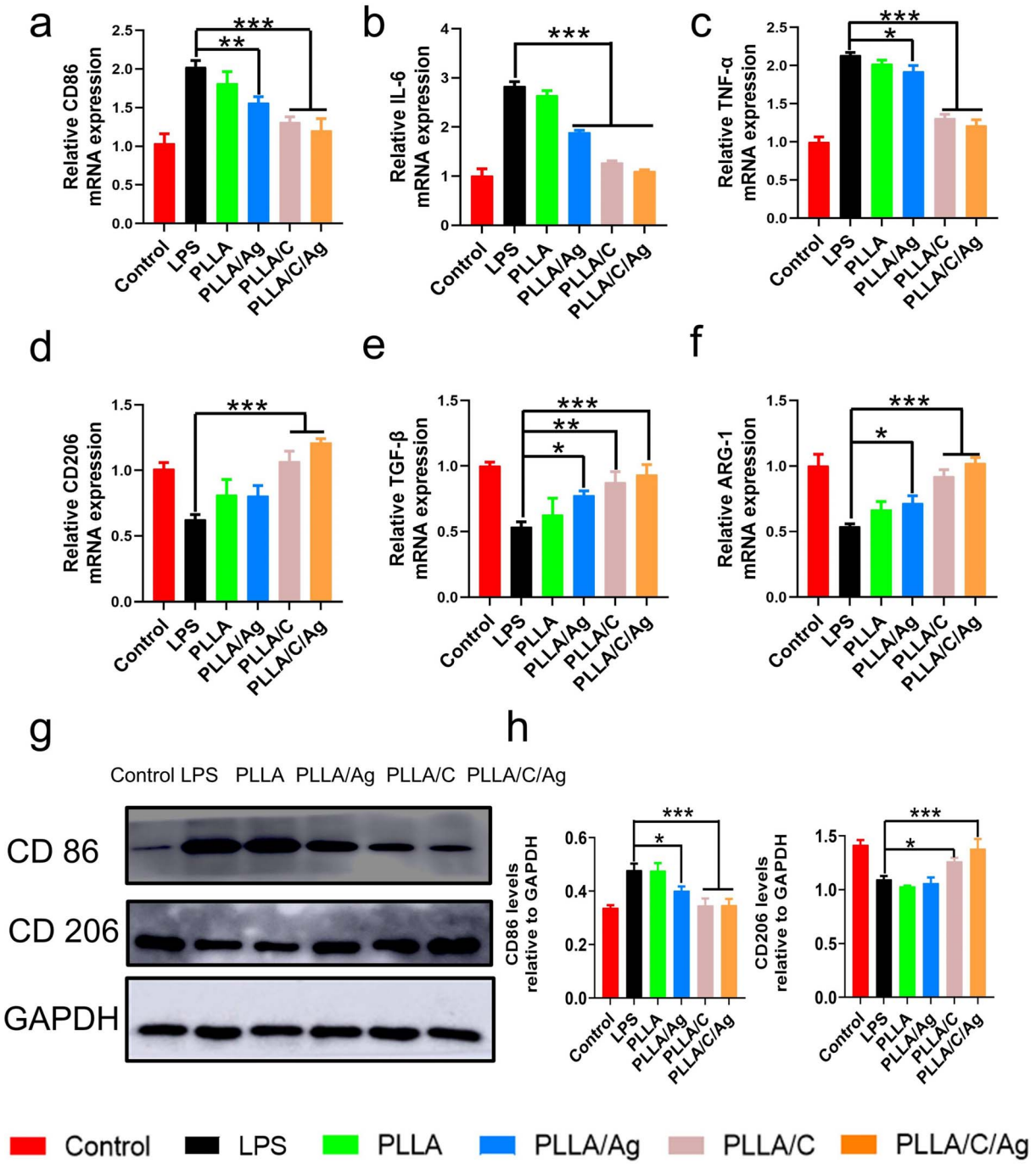

Figure 5. Treatment with PLLA nanofibrous membranes promoted the polarization of macrophages toward the M2 phenotype. (**a**–**f**) The mRNA expression of genes was measured via qRT-PCR. (**g**, **h**) Expression of CD86 and CD206 in macrophages evaluated via western blotting. Data are expressed as the mean ± SD (n = 3) (*$p < 0.05$; **$p < 0.01$; ***$p < 0.001$). *PLLA* poly(L-lactic acid), *PLLA/C* poly(L-lactic acid)/curcumin, *PLLA/Ag* poly(L-lactic acid)/silver nanoparticles, *PLLA/C/Ag* poly(L-lactic acid)/curcumin/silver nanoparticles, *IL-6* interleukin 6, *TNF-α* tumor necrosis factor α, *TGF-β* transforming growth factor β, *ARG-1* arginase 1, *LPS* lipopolysaccharide, *GAPDH* glyceraldehyde-3-phosphate dehydrogenase, *qRT-PCR* quantitative real-time polymerase chain reaction, *SD* standard deviation

can effectively inhibit the production of proinflammatory cytokines in macrophages and facilitate the polarization of macrophages towards the anti-inflammatory (M2) phenotype.

Effects of the nanofibrous membranes on autophagic flux in macrophages Figure 6a, b shows that treatment with the PLLA/Ag, PLLA/C and PLLA/C/Ag membranes increased the LC3-II/I ratio but decreased the expression of P62. To observe

Downloaded from academic.oup.com/burnstrauma/article/doi/10.1093/burnst/tkae009/7687763 by guest on 13 October 2026

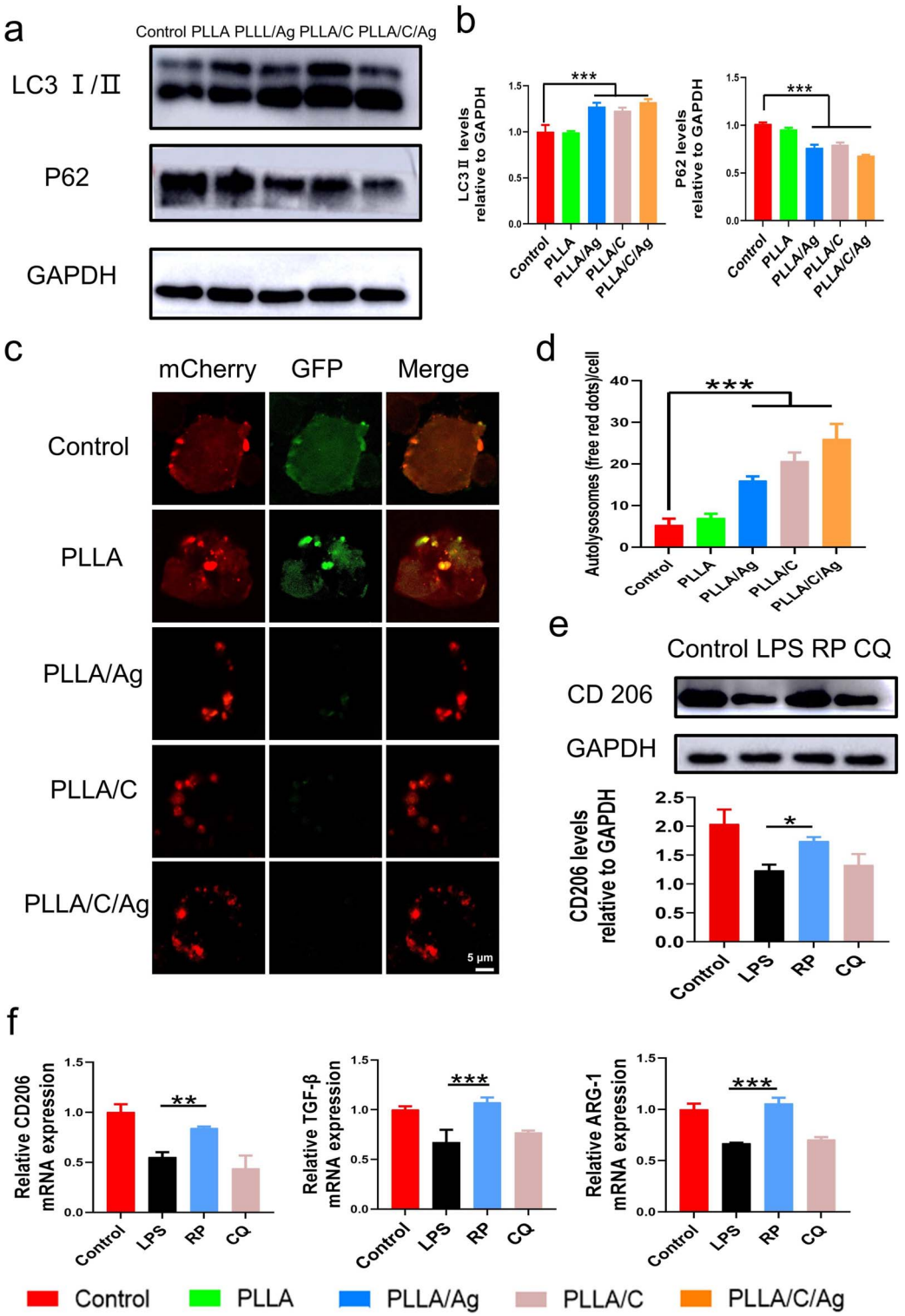

Figure 6. Effects of nanofibrous membranes on autophagic flux in macrophages. (**a**) Western blotting of LC3-I, LC3-II and P62 in RAW264.7 cells treated with nanofibrous membranes. (**b**) Quantitative analysis of western blotting of LC3-I, LC3-II and P62 in RAW264.7 cells treated with nanofibrous membranes. (**c**) Representative immunofluorescence images and quantitative analysis of the number of yellow autophagosomes (G^+R^+) and red autolysosomes (G^-R^+) in mRFP-GFP-LC3 dots in macrophages. (scale bar: 5 μm) (**d**) Autophagic flux was measured by counting the cells with yellow autophagosomes and red autolysosomes. A total of 20 cells were counted per sample for each condition. Data are expressed as mean ± SD (n = 20). (**e**) Representative images and quantitative analysis of western blotting of CD206 in RAW 264.7 cells treated with LPS, rapamycin and chloroquine. (**f**) The mRNA expression of anti-inflammatory molecules in RAW 264.7 cells was analyzed via qRT–PCR. Data are expressed as the mean ± SD (n = 3) (* $p < 0.05$; ** $p < 0.01$; *** $p < 0.001$). *PLLA* poly(L-lactic acid), *PLLA/C* poly(L-lactic acid)/curcumin, *PLLA/Ag* poly(L-lactic acid)/silver nanoparticles, *PLLA/C/Ag* poly(L-lactic acid)/curcumin/silver nanoparticles, *GAPDH* glyceraldehyde-3-phosphate dehydrogenase, *LC3* microtubule-associated proteins light chain 3, *P62* sequestosome 1, *RP* rapamycin, *CQ* chloroquine, *qRT-PCR* quantitative real-time polymerase chain reaction, *mRFP* monomeric red fluorescent protein, *GFP* green fluorescent protein, *SD* standard deviation

Downloaded from academic.oup.com/burnstrauma/article/doi/10.1093/burnst/tkae009/7687763 by guest on 13 October 2026

the effects of the nanofibrous membranes on autophagic flux in macrophages, RAW 264.7 cells were transfected with mCherry-GFP-LC3 adenovirus for 24 h and subsequently treated with nanofibrous membranes for another 24 h. Owing to the instability and quenching of GFP under acidic conditions, only red fluorescent puncta were detectable at this stage. Consequently, the autophagosomes in cells were labelled as yellow dots (where the green and red fluorescence overlapped), whereas autophagolysosomes were labelled as red dots (a result of the quenching of green fluorescence). Confocal microscopy was used to detect mCherry- and GFP-positive dots (Figure 6c). The results demonstrated that the number of red (G^-R^+) dots was substantially increased after treatment with the PLLA/C, PLLA/Ag and PLLA/C/Ag membranes, indicating that the autophagosomes in these cells fused with lysosomes to form autolysosomes and that autophagic flux was activated. However, yellow dots (G^+R^+) were diffusely distributed in the cytoplasm and a few green dots (G^-R^+) were observed in the cells of the control and PLLA groups (Figure 6d). These findings suggest that the PLLA/C/Ag membranes increased the formation of autophagolysosomes by activating autophagic flux in cocultured macrophages.

Considering that the PLLA nanofibrous membranes facilitated the polarization of macrophages and enhanced autophagic flow, our study aimed to explore whether inducing autophagy could stimulate the polarization of macrophages towards the M2 phenotype. As shown in Figure 6e, after being treated with LPS, the expression of CD206 in macrophages was reduced, indicating a shift in macrophage polarization towards the M1 phenotype. After treatment with rapamycin (an autophagy inducer), the expression of CD206 increased substantially, whereas chloroquine (an autophagy inhibitor) administration did not affect the expression of CD206. In contrast, the expression of CD206, TGF-β and ARG-1 genes in LPS-treated macrophages was notably enhanced by rapamycin, while chloroquine had no impact on their mRNA levels (Figure 6f). In addition, rapamycin and chloroquine did not affect the protein or gene expression of M1 macrophage markers (data not shown). These results demonstrate that LPS treatment can polarize macrophages towards the M1 phenotype and that autophagy activation can induce the polarization of macrophages to the M2 phenotype.

In vivo wound healing assessments

Wound healing assessment The wound healing capacity of the PLLA nanofibre sheets was evaluated in a diabetic mouse model with skin wounds of full thickness (Figure 7a). Figure 7b shows the gross appearances of wounds at different time points. The wound closure rate in all groups increased after 7 days of treatment. The PLLA/C/Ag group exhibited the highest wound closure rate and the most efficient healing, with almost complete closure of the wound and the formation of new skin on day 14. However, wounds in the control and PLLA groups were covered by eschar (Figure 7b, c, f). These materials exhibited some level of wound healing ability as the wounds in the PLLA, PLLA/Ag, PLLA/C and Tegaderm film groups were shorter compared to the control group. Additionally, the wound was shorter in the PLLA/C/Ag group than in the PLLA, PLLA/Ag and Tegaderm film groups, demonstrating the superior wound healing ability of PLLA/C/Ag membranes, which was even better than commonly used clinical excipients (Figure 7f). During diabetic wound healing, the PLLA/C/Ag membrane promoted rapid wound contraction, which indicated its significant effects on skin wound healing.

Histological analysis of regenerated skin tissue To assess the pathological characteristics of wounds treated with various nanofibrous membranes, H&E staining was conducted. Overall, the wound length shortened between days 7 and 14 in all groups, with the PLLA/C/Ag group having the shortest wound (Figure 8a and c). Compared with wounds treated with the other nanofibrous membranes, those treated with the PLLA/C/Ag membranes showed a thicker neo-epidermis with more proliferating keratinocytes on day 7 (Figure 8e). Treatment with the PLLA/C/Ag, PLLA/C and PLLA/Ag membranes resulted in the formation of abundant granulation tissue with more layers that were thicker in the wound gap on day 7. In particular, the PLLA/C/Ag membranes had the best ability to form progranulation tissue (Figure 8f). Better skin repair effects were observed in the PLLA/C/Ag group, followed by the PLLA/Ag, PLLA/C and Tegaderm film groups on day 14. Furthermore, on day 14, the PLLA/C/Ag group exhibited the presence of skin appendages, demonstrating a noteworthy rise in the quantity of dermal appendages within the healing tissue in comparison to the remaining groups (Figure 8g), which indicated that complete skin repair can be achieved after treatment with the PLLA/C/Ag membranes. The H&E staining results indicated that the combination of curcumin and Ag in the PLLA/C/Ag membranes had a synergistic effect on enhancing the healing of diabetic wounds and promoting tissue regeneration. Therefore, these PLLA/C/Ag and PLLA/C membranes can be used to promote wound healing.

Masson's trichrome staining is usually used to delineate cells from the surrounding connective tissue. In this study, Masson staining revealed collagen deposition in the ECM in PLLA/C/Ag-treated wounds (Figure 8b). Furthermore, the dermis layer in the PLLA/Ag, PLLA/C and PLLA/C/Ag groups exhibited a greater production of collagen fibres (stained blue) during the healing of wounds compared to the control and PLLA groups on day 7 (Figure 8b and d). As shown in Figure 8b, d, the control group exhibited increased fibrosis with sparse and disorganized collagen deposition on day 14. However, after treatment with the PLLA/C/Ag membranes, collagen deposition increased, and a high wound closure rate was observed. The collagen fibres in the PLLA/C/Ag group exhibited a mature phenotype with regular alignment and network topology, whereas those in the PLLA/Ag, PLLA/C and Tegaderm film groups were dysplastic and loosely arranged.

Next, the regenerated tissue at the wound site was further examined (Figure 7d). During the early stages of wound

Downloaded from academic.oup.com/burnstrauma/article/doi/10.1093/burnst/tkae009/7687763 by guest on 13 October 2026

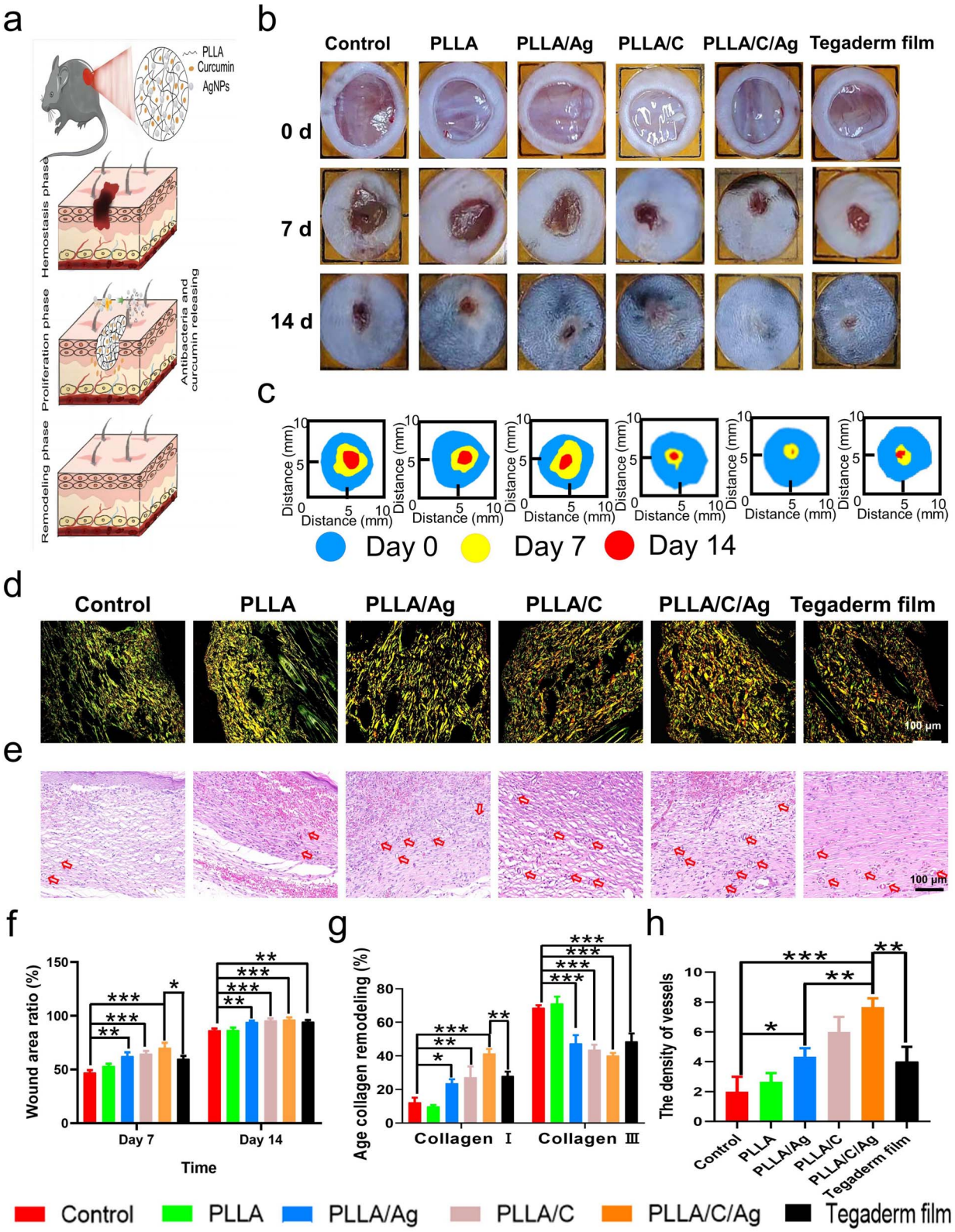

Figure 7. Evaluation of diabetic wound healing *in vivo*. (**a**) Schematic illustration of the treatment process and wound healing *in vivo*. (**b**) Representative images of chronic diabetic wounds treated with different nanofibrous membranes. (**c**) Schematic diagram of wound closure on day 0, 7 and 14 in each group. (**d**) Wound tissues stained with picrosirius red on day 14 were observed under a polarized light microscope. The orange-red colour represents collagen I, whereas the green-yellow colour signifies collagen III (scale bar: 100 μm). (**e**) Representative H&E staining images of blood vessels. Red arrows indicate new vessels (scale bar = 100 μm). (**f**) Quantitative analysis of wound closure in each group. (**g**) Quantification of collagen remodelling on day 14. (**h**) Quantification of the number of vessels. Data are expressed as the mean ± SD (n = 6) (* $p < 0.05$; ** $p < 0.01$; *** $p < 0.001$). *PLLA* poly(L-lactic acid), *PLLA/C* Poly(L-lactic acid)/curcumin, *PLLA/Ag* poly(L-lactic acid)/silver nanoparticles, *PLLA/C/Ag* poly(L-lactic acid)/curcumin/silver nanoparticles, *H&E* hematoxylin and eosin, *SD* standard deviation

Downloaded from academic.oup.com/burnstrauma/article/doi/10.1093/burnst/tkae009/7687763 by guest on 13 October 2026

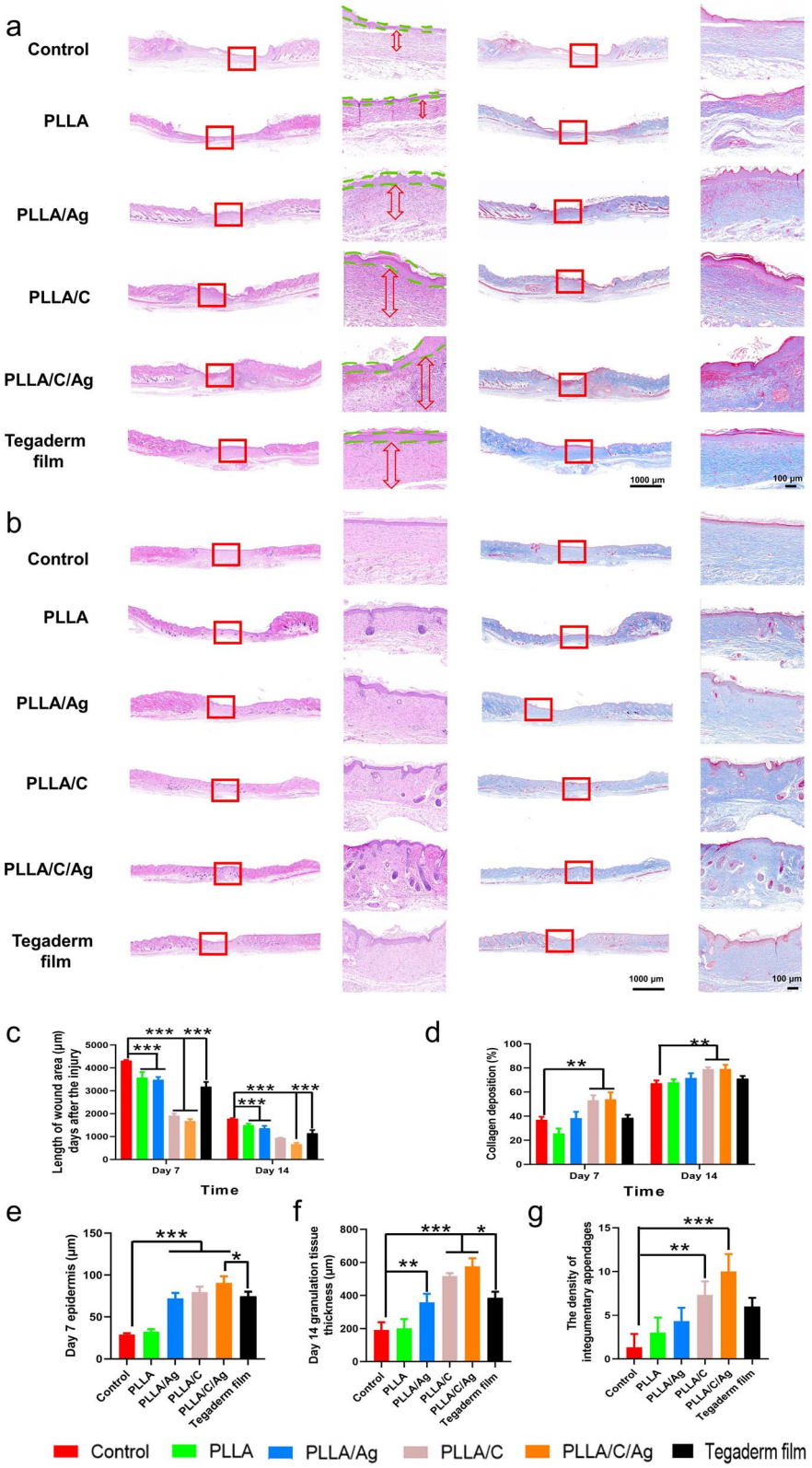

Figure 8. Histological staining. (**a**) Representative H&E and Masson staining of wound tissue samples from different groups on day 7. (**b**) Representative H&E staining and Masson staining of wound tissue samples from different groups on day 14. (Scale bars: 1000 and 100 μm) (**c**) Quantification of the length of wounds on days 7 and 14. (**d**) Quantification of collagen deposition via Masson staining. (**e**) Thickness of the epidermis of wound tissues on day 7. (**f**) Thickness of the granulation tissue of wound tissues on day 7. (**g**) Number of dermal appendages in wound tissues on day 14. Data are expressed as the mean ± SD (n = 6) (* $p < 0.05$; ** $p < 0.01$; *** $p < 0.001$). *PLLA* poly(L-lactic acid), *PLLA/C* poly(L-lactic acid)/curcumin, *PLLA/Ag* poly(L-lactic acid)/silver nanoparticles, *PLLA/C/Ag* poly(L-lactic acid)/curcumin/silver nanoparticles, *H&E* hematoxylin and eosin staining, *SD* standard deviation

Downloaded from academic.oup.com/burnstrauma/article/doi/10.1093/burnst/tkae009/7687763 by guest on 13 October 2026

healing, excessive collagen, mostly collagen type III, is deposited, which covers the wound and prevents further damage [52]. Following tissue remodeling, collagen type I gradually replaces the aforementioned collagen, primarily observed in developed skin [53]. Therefore, we used picrosirius red staining to assess collagen remodelling. Collagen I deposition was increased in the PLLA/C/Ag, PLLA/C, Tegaderm film and PLLA/Ag groups, suggesting that curcumin and Ag had notable impacts on the remodeling of collagen and the maturation of the skin. Consistently, quantification of the amounts of collagen I and III demonstrated that there was enhanced deposition of mature collagen I (Figure 7g) in the PLLA/C/Ag, PLLA/C and PLLA/Ag groups. These results suggest that the sustained release of curcumin and Ag significantly affects collagen remodelling and skin maturation. Furthermore, the PLLA/C/Ag membranes not only facilitate wound healing but also enhance the development of regenerative tissue in the process of diabetic wound healing, a crucial factor for the restoration of intact skin. In addition, the proangiogenic effects induced by the PLLA/A/C membranes may lead to rapid wound healing. The newly formed blood vessels were visualized and quantified on day 7 via H&E staining (Figure 7e). The PLLA/C/Ag, PLLA/C and PLLA/Ag groups showed a notable rise in the quantity of recently developed blood vessels when compared to the control and PLLA groups, as shown in Figure 7h. Therefore, these PLLA/C/Ag membranes can promote angiogenesis in diabetic wounds to facilitate healing.

Immunofluorescence analysis An estimation was made of the quantity of circular arterioles present in the imaging region, along with a count of newly developed blood vessels. To distinguish smooth muscle cells from myofibroblasts, only α-SMA-positive circular structures, which represent newly formed blood vessels, were examined (marked with white arrows in Figure 9a). The PLLA/Ag, PLLA/C and PLLA/C/Ag groups exhibited a significantly greater quantity of arterioles compared to both the control and PLLA groups. Specifically, the PLLA/C and PLLA/C/Ag groups exhibited a notably greater number compared to the PLLA/Ag groups (Figure 9d). Furthermore, wound samples were stained with anti-CD31 antibody to detect capillaries (Figure 9a). In both the PLLA and PLLA/Ag groups, the level of CD31 expression was low, while it was notably elevated in the PLLA/C and PLLA/C/Ag groups compared to the control group (Figure 9e). These results suggest that the PLLA/C/Ag membranes can accelerate wound closure and improve angiogenesis. Consistently, previous studies have reported a positive correlation between the number of blood capillaries and rapid wound healing [54,55].

In order to examine the function of the PLLA nanofibrous membranes in controlling inflammation, immunofluorescence analysis was conducted to assess the expression of CD86 and CD206 (Figure 9b, f, g). In the PLLA/C and PLLA/C/Ag groups, there was a notable decrease in the percentage of M1-type macrophages and a significant increase in the proportion of M2-type macrophages. These results indicate that the PLLA/C and PLLA/C/Ag membranes promote the polarization of macrophages towards the M2 phenotype. Furthermore, our investigation aimed to determine if *in vivo* autophagy can be induced by PLLA/C/Ag membranes. The fluorescence microscopy images indicated that the level of LC3 expression at the wound site was notably greater in the PLLA/C/Ag group compared to the control group (Figure 9c, h). Additionally, the expression of LC3 and P62 in macrophages at the wound site was examined via western blotting (Figure 9i–k). The results showed that there was an augmentation in LC3 expression and a reduction in P62 expression, suggesting the initiation of autophagy.

Discussion

Diabetic wounds, in contrast to typical wounds, are characterized by their susceptibility to chronicity due to the presence of oxidative stress, infection and inflammation. In the present study, a PLLA nanofibre membrane incorporating curcumin and AgNPs was found to enhance the proliferation of granulation tissue and the deposition of collagen in skin wounds of diabetic mice. This effect was attributed to the membrane's anti-inflammatory, antioxidant and antibacterial properties, ultimately expediting the healing process of diabetic wounds.

Air-jet spinning is widely used to prepare biodegradable nanofibrous membranes owing to its rapid nature, convenience, low cost and safety [56]. In this study, air-jet spinning was employed to fabricate PLLA nanofibrous membranes, and curcumin was efficiently encapsulated in the nanofibrous membranes owing to its hydrophobicity and good solubility in methylene chloride. Subsequently, AgNPs were successfully encapsulated into the membranes via the *in situ* chemical reduction of $AgNO_3$ using tannic acid as the reducing agent. To introduce certain amino groups onto the surface of the nanofibrous membranes, ammonia plasma treatment was performed. The introduced amino groups could graft tannic acid onto the surface of the nanofibrous membranes with glutaraldehyde through aldehyde–amine and aldehyde–hydroxy reactions [57]. Tannic acid, with its multiple phenolic hydroxyl groups and highly potent reducing activity, facilitated the *in situ* chemical reduction of $AgNO_3$ to form AgNPs.

The FTIR spectra of all nanofibrous membranes showed the presence of two absorption peaks at 1749 and 1084 cm^{-1}, which can be attributed to the stretching vibrations of C=O and C–O in PLLA, respectively. Furthermore, the structures of the nanofibrous membranes remained unchanged after the introduction of amino groups via ammonia plasma treatment and the incorporation of curcumin. It should be noted that the height of the FTIR surface measurement was ~500 nm, while that of the plasma-treated membrane surface was only 5–50 nm. Therefore, the new groups introduced by ammonia plasma treatment may not be detected by this method, and instead, only the functional groups of the membranes were detected. After treatment, the contact angles of the PLLA and PLLA/C membranes decreased by 40.1 and 38.6%

Downloaded from academic.oup.com/burnstrauma/article/doi/10.1093/burnst/tkae009/7687763 by guest on 13 October 2026

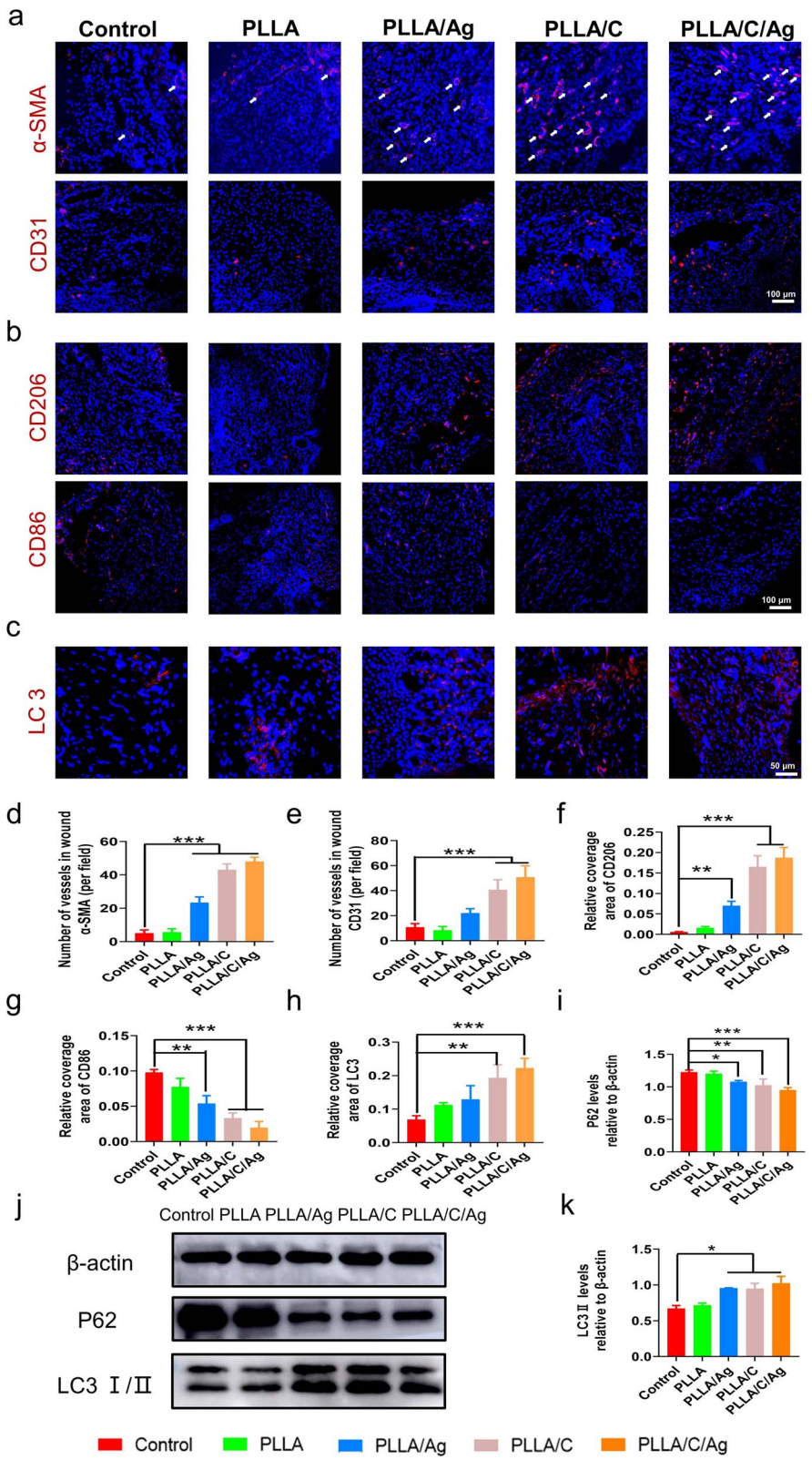

Figure 9. Immunofluorescence analysis in the diabetic wound model 14 days after surgery. (**a**) Immunohistochemical analysis of α-SMA and CD31 in skin wound samples (scale bar: 100 μm). (**b**) Immunohistochemical analysis of CD86 and CD206 in skin wound samples (scale bar: 100 μm). (**c**) Immunohistochemical analysis of LC3 in skin wound samples (scale bar: 50 μm). (**d**–**h**) Quantification of the results of immunohistochemical analysis. (**i**–**k**) Western blotting of LC3-I, LC3-II and P62 in macrophages in mice treated with PLLA nanofibrous membranes. Data are expressed as the mean ± SD (n = 3) (* $p < 0.05$; ** $p < 0.01$; *** $p < 0.001$). *PLLA* poly(L-lactic acid), *PLLA/C* poly(L-lactic acid)/curcumin, *PLLA/Ag* poly(L-lactic acid)/silver nanoparticles, *PLLA/C/Ag* poly(L-lactic acid)/curcumin/silver nanoparticles, *α-SMA* alpha-smooth muscle actin, *β-actin* beta-actin, *LC3* microtubule-associated proteins light chain 3, *SD* standard deviation

Downloaded from academic.oup.com/burnstrauma/article/doi/10.1093/burnst/tkae009/7687763 by guest on 13 October 2026

respectively. These decreases in water contact angles indicated that the hydrophilicity of the membranes was improved [58]. Moreover, the contact angle of the PLLA/C/Ag film that underwent Ag nanoparticle grafting measured $63.2 \pm 4.4°$, exhibiting a reduction of 16.2° compared to the contact angle of the PLLA/C/N film. This emphasizes the substantial improvement in the hydrophilicity of the grafted substance. Moreover, the utilization of XPS examination enabled the identification of C–N–H and C=N–C clusters on the PLLA/N nanofibrous membrane's surface, exhibiting a nitrogen composition of 2.97%. Collectively, these results suggest that ammonia plasma treatment is a convenient and efficient method for introducing hydrophilic amino groups onto the surface of PLLA nanofibrous membranes.

Enhancing the water affinity of PLLA membranes promotes the attachment, development and multiplication of dermal cells on the membranes [59]. To enhance the hydrophilicity of PLLA-based nanofibrous membranes, the surface of the membrane is typically subjected to chemical grafting or hydrolysis, which introduces new substances or damages the structure of the membrane to a certain extent [60,61]. However, ammonia plasma treatment offers a convenient and inexpensive approach that allows for the prompt introduction of hydrophilic groups without compromising the structure of the material [62,63]. According to the XRD results, a diffraction peak at 44.52°, corresponding to the (200) crystallographic plane of the Ag face-centred cubic crystal structure [48], was observed in the PLLA/Ag and PLLA/C/Ag film samples but not in the samples of the PLLA and PLLA/C films, indicating the presence of AgNPs in the former PLLA films and further confirming the successful *in situ* chemical reduction of $AgNO_3$ using tannic acid as the reducing agent. The large surface area of the nanofibrous membranes improves their interaction with tissue, enabling continuous drug release [64]. The burst release of curcumin in the initial stage can contribute to the anti-inflammatory effects of the membranes during the early stage of wound healing. We speculate that this burst release can be attributed to the surface distribution of curcumin in the membranes accomplished by air-jet spinning [65,66]. Furthermore, the release of AgNPs gradually increased, providing a certain bactericidal effect. This is likely due to the gradual release of AgNPs embedded in the PLLA membrane, which effectively mitigates their toxicity during the release process. Compared to a recent study [67], our loading and release processes are similar, but the concentration of released AgNPs is even lower, which may result in lower biological toxicity.

The skin is constantly exposed to the external environment and needs to have good elasticity and mechanical properties to withstand daily activities. Therefore, wound dressings must possess sufficient mechanical and adhesive properties to meet these requirements. The PLLA/C/Ag membrane demonstrates favourable mechanical properties, including flexibility and the ability to bend and fold, which can be adjusted based on the affected area. This membrane also exhibits significant water absorption ability, making it suitable for absorbing exudate from diabetic wounds. During the diabetic wound healing process, the exudation of tissue fluid is common, making the expansion capability of the biofilm crucial. The PLLA/C/Ag membrane itself possesses a remarkable water absorption ability, with an absorption rate that initially increases and then gradually decreases. This membrane can expand up to 2–3 times its original volume, making it highly effective in absorbing exudate from the wound area.

It is critical that wound dressings are biocompatible, as they need to be in close contact with body tissues. The excellent compatibility of the nanofibrous filters was proven through the growth and movement of cocultured NIH-3T3 fibroblasts. The presence of AgNPs and curcumin, as well as the hydrophilicity of the membranes, played significant roles in promoting cell proliferation. AgNPs can have varying cytotoxicity depending on their size, surface properties and the cell line they are tested with, while curcumin is generally considered nontoxic to the body and various cell lines. One advantage of PLLA nanofibrous membranes is their ability to sustain the delivery of bioactive substances, preventing toxic effects due to overdose. The hydrophilicity of the membranes was greatly improved after ammonia plasma treatment. Moreover, the PLLA nanofibre sheets enclosing curcumin (PLLA/C and PLLA/C/Ag) greatly improved the migratory capacity of NIH-3T3 cells, in line with prior research. Overall, these findings strongly indicate that the PLLA nanofibrous membranes have minimal toxicity and can serve as highly biocompatible wound dressings to promote wound healing.

Compared to other types of wounds, diabetic wounds have a slower healing process and tend to produce more exudates, which increase the risk of bacterial infection and delay wound healing [66]. Therefore, wound dressings for diabetic wounds should possess inherent antibacterial properties to prevent external bacterial infections, as the use of conventional antibiotics can contribute to bacterial resistance [68]. The exceptional antibacterial efficacy of the membranes produced in this study, both *in vitro* and *in vivo*, is attributed to the highly potent antibacterial properties of AgNPs. The antibacterial activity of AgNPs can be attributed to the following three elucidated mechanisms. First, AgNPs can penetrate the outer membrane of bacteria, increasing membrane permeability and leading to the leakage of cellular contents and ultimately cell death [69,70]. Second, AgNPs have an affinity for the sulfur or phosphorus groups present in intracellular components such as DNA and proteins, and thus the AgNPs can alter the structure and function of these components [50,71–73]. Third, the silver ions released from AgNPs can interact with cellular components such as membranes and nucleic acids [50,71–73]. Moreover, AgNPs embedded in wound dressings, such as hydrogels and nanofibrous membranes, can also exhibit bacteriostatic effects [72,73]. Although *Pseudomonas aeruginosa* is a common bacterium found in diabetic foot ulcers [74,75], we were unable to test the fabricated nanofibrous membranes against *P. aeruginosa*. However, a study

Downloaded from academic.oup.com/burnstrauma/article/doi/10.1093/burnst/tkae009/7687763 by guest on 13 October 2026

by Pourmbarak Mahnaie *et al.* reported the effectiveness of AgNPs against *P. aeruginosa* [76].

Persistent hyperglycemia, infection and an activated immune system contribute to the build-up of ROS in diabetic wounds, resulting in heightened oxidative stress, prolonged inflammation and impaired wound healing [77]. The treatment of diabetic wounds can be improved by focusing on reducing oxidative stress, as suggested in a previous study [78]. Wound dressings that integrate antioxidants can scavenge ROS, promote enzymatic repair and activate metabolic pathways, thereby facilitating diabetic wound healing [79]. This study revealed that the inclusion of curcumin in the PLLA nanofibrous membranes exhibited a notable capacity to eliminate ROS in both the PLLA/C and PLLA/C/Ag groups. These membranes exhibited potential antioxidant effects, as supported by their ROS scavenging ability and the observed increase in SOD activity [79]. While PLLA nanofibrous membranes encapsulating AgNPs showed moderate antioxidant activity, the combination of AgNPs and curcumin did not exhibit synergistic antioxidant effects. These findings suggest that PLLA nanofibrous membranes may serve as effective wound dressings for diabetic wounds with elevated ROS levels.

Macrophages have a vital function in the alteration of tissues and can display either proinflammatory (M1) or anti-inflammatory (M2) characteristics [80]. Promoting the shift of macrophages from the proinflammatory M1 phenotype to the anti-inflammatory M2 phenotype is advantageous for the healing of persistent wounds [81]. Activation of Toll-like receptor 4 by LPS leads to the release of inflammatory substances and the infiltration of macrophages that produce proinflammatory cytokines, thereby causing a delay in the healing process of wounds [82]. In this study, treatment with the PLLA/Ag, PLLA/A/C and PLLA/C/Ag membranes inhibited the expression of proinflammatory cytokines in macrophages and promoted macrophage polarization towards the M2 phenotype. These findings suggest that the PLLA/Ag, PLLA/A/C and PLLA/C/Ag membranes exert immunosuppressive effects by promoting M2 macrophage polarization, which may alleviate diabetic wounds and promote healing.

Autophagy, a critical regulatory process in macrophage polarization, decreases inflammation [83]. Autophagy down-regulates the inflammasome, which promotes the production of active inflammatory cytokines during inflammation [84]. Previous research has reported that autophagy induced by cathepsins and IL-6 promotes M2 polarization, while inhibiting autophagy can restore Nuclear factor kappa-B (NF-κB) activity and stimulate M2 polarized macrophages to produce M1-like cytokines [18,85]. In this study, it was demonstrated that PLLA nanofibrous membranes can induce M2 macrophage polarization by activating autophagy. The modulation of autophagy and M2 polarization by the PLLA nanofibrous membranes may attenuate inflammation and facilitate wound healing.

Delayed wound healing in diabetic patients is attributed to prolonged inflammation, impaired angiogenesis and delayed wound closure, with sustained inflammation playing a significant role in impairing early healing responses [86]. In diabetic wounds, resident macrophages tend to remain in the proinflammatory (M1) state for an extended period, highlighting the importance of promoting the M1-to-M2 phase transition for chronic wound healing [87]. Activating autophagy is a promising strategy for promoting macrophage polarization towards the M2 phenotype and inhibiting inflammation [88]. The findings of this research confirmed that autophagy is induced by PLLA nanofibrous membranes, as demonstrated by the transformation of LC3-I into LC3-II and the breakdown of P62. Furthermore, these membranes polarize macrophages towards the M2 phenotype and inhibit inflammation, and promote angiogenesis, granulation tissue formation, collagen deposition and epithelial cell formation. Modulating the activation of autophagy may be a mechanism through which these PLLA nanofibrous membranes promote diabetic wound healing.

Conclusions

In summary, our findings demonstrated that multifunctional immunomodulatory PLLA nanofibrous membranes have a significant therapeutic effect on wound healing in diabetic mice. This study proved that this therapeutic effect is achieved by inhibiting inflammation, oxidation and bacterial growth. Therefore, these multifunctional immunomodulatory PLLA nanofibrous membranes have the potential to effectively treat diabetic wounds.

Supplementary data

Supplementary data is available at *Burns & Trauma Journal* online.

Abbreviations

α-SMA: α-Smooth muscle actin, AgNPs: Silver nanoparticles; ATGs: Autophagy-related genes; Arg1: Arginase-1; Calcein-AM: Calcein acetoxymethyl ester; CD86: Cluster of differentiation 86; CD206: Cluster of differentiation 206; CFU: Colony-forming units; DAPI: 4,6-Diamino-2-phenyl indole; DMEM: Dulbecco's modified Eagle's medium; DCFH-DA: 2′-7′ Dichlorofluorescein diacetate; DCF: 2,7-Dichloro-fluorescein; ECM: Extracellular matrix; ELISA: Enzyme-linked immunosorbent assay; FTIR: Fourier-transform infrared spectrometry; GFP: Green fluorescent protein; H&E: Hematoxylin and eosin; IL-6: Interleukin 6; LB: Luria–Bertani; LPS: Lipopolysaccharide; MTT: 3-(4,5-Dimethylthiazol-2-yl)-2,5-diphenyltetrazolium bromide; OD: Optical density; PI: Propidium iodide; PLLA: Poly(L-lactic acid poly(L-lactic acid; PLLA/C/Ag: PLLA nanofibrous membranes incorporated with AgNPs and curcumin; PLLA/C: PLLA nanofibrous membranes loaded with curcumin; PLLA/Ag: PLLA nanofibrous membranes loaded with AgNPs; qRT-PCR: Quantitative reverse transcription polymerase chain reaction; ROS: Reactive oxygen species; rpm: Revolutions per minute; SOD: Superoxide dismutase; TNF-α: Tumor necrosis factor-α; TGF-β: Transforming growth factor-beta; XPS: X-Ray photoelectron spectroscopy; XRD: X-Ray diffraction.

Downloaded from academic.oup.com/burnstrauma/article/doi/10.1093/burnst/tkae009/7687763 by guest on 13 October 2026

Funding

This research was supported by the National Natural Science Foundation of China (82072051), the Central Finance Supports Local Colleges, and Universities Talent Development Funding from Heilongjiang Provincial Department of Finance (2020GSP09), the Natural Science Foundation of Heilongjiang Province (LH2020H076) and Mudanjiang City Guiding Science and Technology Plan Project (HT2022JG125).

Authors' contributions

YW: Conceptualization, validation, investigation, formal analysis, writing–original draft. JZ and AQL: Methodology, writing–original draft. TLZ, CLZ, YKY and RG: Methodology. YL: Validation. JG: Conceptualization, funding acquisition, project administration, writing–review and editing. YLL: Funding acquisition, supervision. YHC: Funding acquisition, project administration, writing–original draft, writing–review and editing.

Conflict of interest

None declared.

References

1. Sun H, Saeedi P, Karuranga S, Pinkepank M, Ogurtsova K, Duncan BB, *et al*. IDF Diabetes Atlas: Global, regional and country-level diabetes prevalence estimates for 2021 and projections for 2045. *Diabetes Res Clin Pract*. 2022;183:109119. https://doi.org/10.2337/diacare.27.5.1047.
2. Gurtner GC, Werner S, Barrandon Y, Longaker MT. Wound repair and regeneration. *Nature*. 2008;453:314–21.
3. Zhao R, Liang H, Clarke E, Jackson C, Xue M. Inflammation in chronic wounds. *Int J Mol Sci*. 2016;17:E2085.
4. Liu H, Qu X, Kim E, Lei M, Dai K, Tan X, *et al*. Bio-inspired redox-cycling antimicrobial film for sustained generation of reactive oxygen species. *Biomaterials*. 2018;162:109–22.
5. Shen Y-I, Cho H, Papa AE, Burke JA, Chan XY, Duh EJ, *et al*. Engineered human vascularized constructs accelerate diabetic wound healing. *Biomaterials*. 2016;102:107–19.
6. Chen L, Xing Q, Zhai Q, Tahtinen M, Zhou F, Chen L, *et al*. Pre-vascularization enhances therapeutic effects of human mesenchymal stem cell sheets in full thickness skin wound repair. *Theranostics*. 2017;7:117–31.
7. Freudenberg U, Zieris A, Chwalek K, Tsurkan MV, Maitz MF, Atallah P, *et al*. Heparin desulfation modulates VEGF release and angiogenesis in diabetic wounds. *J Control Release Off J Control Release Soc*. 2015;220:79–88.
8. Choi SM, Lee K-M, Kim HJ, Park IK, Kang HJ, Shin H-C, *et al*. Effects of structurally stabilized EGF and bFGF on wound healing in type I and type II diabetic mice. *Acta Biomater*. 2018;66:325–34.
9. Losi P, Briganti E, Errico C, Lisella A, Sanguinetti E, Chiellini F, *et al*. Fibrin-based scaffold incorporating VEGF- and bFGF-loaded nanoparticles stimulates wound healing in diabetic mice. *Acta Biomater*. 2013;9:7814–21.
10. Kant V, Kumar D, Prasad R, Gopal A, Pathak NN, Kumar P, *et al*. Combined effect of substance P and curcumin on cutaneous wound healing in diabetic rats. *J Surg Res*. 2017;212:130–45.
11. Hamed S, Ullmann Y, Egozi D, Daod E, Hellou E, Ashkar M, *et al*. Fibronectin potentiates topical erythropoietin-induced wound repair in diabetic mice. *J Invest Dermatol*. 2011;131:1365–74.
12. Lee C-H, Hung K-C, Hsieh M-J, Chang S-H, Juang J-H, Hsieh I-C, *et al*. Core-shell insulin-loaded nanofibrous scaffolds for repairing diabetic wounds. *Nanomedicine Nanotechnol Biol Med*. 2020;24:102123.
13. Alexis F. Factors affecting the degradation and drug-release mechanism of poly(lactic acid) and poly[(lactic acid)-co-(glycolic acid)]. *Polym Int*. 2005;54:36–46.
14. Daristotle JL, Behrens AM, Sandler AD, Kofinas P. A review of the fundamental principles and applications of solution blow spinning. *ACS Appl Mater Interfaces*. 2016;8:34951–63.
15. Sinha-Ray S, Sinha-Ray S, Yarin AL, Pourdeyhimi B. Theoretical and experimental investigation of physical mechanisms responsible for polymer nanofiber formation in solution blowing. *Polymer*. 2015;56:452–63.
16. Rahmati M, Mills DK, Urbanska AM, Saeb MR, Venugopal JR, Ramakrishna S, *et al*. Electrospinning for tissue engineering applications. *Prog Mater Sci*. 2021;117:100721.
17. Zhang S, Li Y, Qiu X, Jiao A, Luo W, Lin X, *et al*. Incorporating redox-sensitive nanogels into bioabsorbable nanofibrous membrane to acquire ROS-balance capacity for skin regeneration. *Bioact Mater*. 2021;6:3461–72.
18. Cui S, Sun X, Li K, Gou D, Zhou Y, Hu J, *et al*. Polylactide nanofibers delivering doxycycline for chronic wound treatment. *Mater Sci Eng C Mater Biol Appl*. 2019;104:109745 https://pubmed.ncbi.nlm.nih.gov/31499963/.
19. Thönes S, Rother S, Wippold T, Blaszkiewicz J, Balamurugan K, Moeller S, *et al*. Hyaluronan/collagen hydrogels containing sulfated hyaluronan improve wound healing by sustained release of heparin-binding EGF-like growth factor. *Acta Biomater*. 2019;86:135–47.
20. Zhan J, Xu H, Zhong Y, Wu Q, Liu Z. Surface modification of patterned electrospun nanofibrous films via the adhesion of DOPA-bFGF and DOPA-ponericin G1 for skin wound healing. *Mater Des*. 2020;188:108432.
21. Vitiello D, Neagoe P-E, Sirois MG, White M. Effect of everolimus on the immunomodulation of the human neutrophil inflammatory response and activation. *Cell Mol Immunol*. 2015;12:40–52.
22. Jurenka JS. Anti-inflammatory properties of curcumin, a major constituent of Curcuma longa: a review of preclinical and clinical research. *Altern Med Rev J Clin Ther*. 2009;14:141–53.
23. Teymouri M, Pirro M, Johnston TP, Sahebkar A. Curcumin as a multifaceted compound against human papilloma virus infection and cervical cancers: a review of chemistry, cellular, molecular, and preclinical features. *BioFactors Oxf Engl*. 2017;43:331–46.
24. Panahi Y, Khalili N, Sahebi E, Namazi S, Simental-Mendía LE, Majeed M, *et al*. Effects of Curcuminoids plus Piperine on Glycemic, hepatic and inflammatory biomarkers in patients with type 2 diabetes mellitus: a randomized double-blind placebo-controlled trial. *Drug Res*. 2018;68:403–9.
25. Akbik D, Ghadiri M, Chrzanowski W, Rohanizadeh R. Curcumin as a wound healing agent. *Life Sci*. 2014;116:1–7.
26. Sohn S-I, Priya A, Balasubramaniam B, Muthuramalingam P, Sivasankar C, Selvaraj A, *et al*. Biomedical applications and bioavailability of curcumin-an updated overview. *Pharmaceutics*. 2021;13:2102.
27. Guo X, Zhu X, Liu D, Gong Y, Sun J, Dong C. Continuous delivery of propranolol from liposomes-in-microspheres significantly inhibits infantile hemangioma growth. *Int J Nanomedicine*. 2017;Volume 12:6923–36.

Downloaded from academic.oup.com/burnstrauma/article/doi/10.1093/burnst/tkae009/7687763 by guest on 13 October 2026

28. Liu S, Zhang Q, Yu J, Shao N, Lu H, Guo J, *et al.* Absorbable Thioether grafted hyaluronic acid Nanofibrous hydrogel for synergistic modulation of inflammation microenvironment to accelerate chronic diabetic wound healing. *Adv Healthc Mater*. 2020;9:e2000198.
29. Li Y, Leng Q, Pang X, Shi H, Liu Y, Xiao S, *et al.* Therapeutic effects of EGF-modified curcumin/chitosan nano-spray on wound healing. *Regen Biomater*. 2021;8:rbab009.
30. Chaushu L, Rahmanov Gavrielov M, Chaushu G, Zar K, Vered M. Curcumin promotes primary oral wound healing in a rat model. *J Med Food*. 2021;24:422–30.
31. Punjataewakupt A, Napavichayanun S, Aramwit P. The downside of antimicrobial agents for wound healing. *Eur J Clin Microbiol Infect Dis Off Publ Eur Soc Clin Microbiol*. 2019;38:39–54.
32. Rams TE, Degener JE, van Winkelhoff AJ. Antibiotic resistance in human chronic periodontitis microbiota. *J Periodontol*. 2014;85:160–9.
33. Dodwad V, Vaish S, Mahajan A, Chhokra M. Local drug delivery in periodontics: a strategic intervention. *Int J Pharm Pharm Sci*. 2012;4:30–4.
34. Konop M, Damps T, Misicka A, Rudnicka L. Certain aspects of silver and silver nanoparticles in wound care: a Minireview. *J Nanomater*. 2016;2016:e7614753, 1–10.
35. Rai MK, Deshmukh SD, Ingle AP, Gade AK. Silver nanoparticles: the powerful nanoweapon against multidrug-resistant bacteria. *J Appl Microbiol*. 2012;112:841–52.
36. Kharaziha M, Baidya A, Annabi N. Rational Design of Immunomodulatory Hydrogels for chronic wound healing. *Adv Mater Deerfield Beach Fla*. 2021;33:e2100176.
37. Takahama M, Akira S, Saitoh T. Autophagy limits activation of the inflammasomes. *Immunol Rev*. 2018;281:62–73.
38. Cao C, Ren Z, Tan Y. Punicalagin prevents inflammation in LPS-induced RAW264.7 macrophages by inhibiting FoxO3a/autophagy Signaling pathway. *Nutrients*. 2019;11:2794.
39. Zhang S, Xie F, Li K, Zhang H, Yin Y, Yu Y, *et al.* Gold nanoparticle-directed autophagy intervention for antitumor immunotherapy via inhibiting tumor-associated macrophage M2 polarization. *Acta Pharm Sin B*. 2022;12:3124–38.
40. Tu Z, Jiang X, Li Y, Yang S, Lin D, Shi Y, *et al.* Curcumin promotes the survival of ischemic random skin flaps via autophagy. *Am J Transl Res*. 2021;13:1337–51.
41. Shang M, Chang X, Niu S, Li J, Zhang W, Wu T, *et al.* The key role of autophagy in silver nanoparticle-induced BV2 cells inflammation and polarization. *Food Chem Toxicol*. 2021;154:112324.
42. Liao HT, Lai Y-T, Kuo C-Y, Chen J-P. A bioactive multifunctional heparin-grafted aligned poly(lactide-co-glycolide)/curcumin nanofiber membrane to accelerate diabetic wound healing. *Mater Sci Eng C Mater Biol Appl*. 2021;120:111689.
43. Sahu A, Jeon J, Lee MS, Yang HS, Tae G. Antioxidant and anti-inflammatory activities of Prussian blue nanozyme promotes full-thickness skin wound healing. *Mater Sci Eng C*. 2021;119:111596.
44. Wang C, Wang M, Xu T, Zhang X, Lin C, Gao W, *et al.* Engineering bioactive self-healing antibacterial exosomes hydrogel for promoting chronic diabetic wound healing and complete skin regeneration. *Theranostics*. 2019;9:65–76.
45. Yang Y, Zhao X, Yu J, Chen X, Wang R, Zhang M, *et al.* Bioactive skin-mimicking hydrogel band-aids for diabetic wound healing and infectious skin incision treatment. *Bioact Mater*. 2021;6:3962–75.
46. Yuan X, Yang W, Fu Y, Tao Z, Xiao L, Zheng Q, *et al.* Four-arm polymer-guided formation of curcumin-loaded flower-like porous microspheres as injectable cell carriers for diabetic wound healing. *Adv Healthc Mater*. 2023;12:e2301486.
47. Sharma S, Majumdar A, Butola BS. Tailoring the biodegradability of polylactic acid (PLA) based films and ramie- PLA green composites by using selective additives. *Int J Biol Macromol*. 2021;181:1092–103.
48. Baran A, Fırat Baran M, Keskin C, Hatipoğlu A, Yavuz Ö, İrtegün Kandemir S, *et al.* Investigation of antimicrobial and cytotoxic properties and specification of silver nanoparticles (AgNPs) derived from Cicer arietinum L. green leaf extract. Front Bioeng. *Biotechnol*. 2022;10:10.
49. Moran GJ, Krishnadasan A, Gorwitz RJ, Fosheim GE, McDougal LK, Carey RB, *et al.* Methicillin-resistant S. Aureus infections among patients in the emergency department. *N Engl J Med*. 2006;355:666–74.
50. Uddin I, Parimi DS, Bollu TK, Bhatt CS, Suresh AK. Silver Nanoparticles as Potent Multidrug-Resistant Incorporants in Biomedicine. In: Akhtar N, Singh KS, Prerna, Goyal D (eds). *Emerg Modalities Mitig Antimicrob Resist*. Cham: Springer International Publishing, 2022, 475–88.
51. Ding X, Peng F, Zhou J, Gong W, Slaven G, Loh KP, *et al.* Defect engineered bioactive transition metals dichalcogenides quantum dots. *Nat Commun*. 2019;10:41.
52. Girardi M, Lewis J, Glusac E, Filler RB, Geng L, Hayday AC, *et al.* Resident skin-specific gammadelta T cells provide local, nonredundant regulation of cutaneous inflammation. *J Exp Med*. 2002;195:855–67.
53. Chen B, Li R, Yan N, Chen G, Qian W, Jiang H-L, *et al.* Astragaloside IV controls collagen reduction in photoaging skin by improving transforming growth factor-β/Smad signaling suppression and inhibiting matrix metalloproteinase-1. *Mol Med Rep*. 2015;11:3344–8.
54. Chen H, Cheng R, Zhao X, Zhang Y, Tam A, Yan Y, *et al.* An injectable self-healing coordinative hydrogel with antibacterial and angiogenic properties for diabetic skin wound repair. *NPG Asia Mater*. 2019;11:1–12.
55. Bhang SH, Jang WS, Han J, Yoon J-K, La W-G, Lee E, *et al.* Zinc oxide Nanorod-based piezoelectric dermal patch for wound healing. *Adv Funct Mater*. 2017;27:1603497.
56. Liaw C-Y, Huynh S, Gedeon C, Ji S, D'souza C, Abaci A, *et al.* Airbrushed nanofibrous membranes to control stem cell infiltration in 3D-printed scaffolds. *AICHE J*. 2021;67:e17475.
57. Zulys A, Yulia F, Muhadzib N, Nasruddin. Biological metal–organic frameworks (bio-MOFs) for CO2 capture. *Ind Eng Chem Res*. 2021;60:37–51.
58. Ghorabi S, Ashtiani FZ, Karimi M, Fouladitajar A, Yousefi B, Dorkalam F. Development of a novel dual-bioinspired method for synthesis of a hydrophobic/hydrophilic polyethersulfone coated membrane for membrane distillation. *Desalination*. 2021;517:115242.
59. Liang B, Feng T, Yuan X, Zhao K, Li C, Han Y. Proportion-dependent osteogenic activity of electrospun nano-hydroxyapatite/polylactic acid fiber membrane in vitro and in vivo. *Mater Des*. 2022;219:110834.
60. Xiong Z, Lin H, Liu F, Yu X, Wang Y, Wang Y. A new strategy to simultaneously improve the permeability, heat-deformation resistance and antifouling properties of polylactide membrane via bio-based β-cyclodextrin and surface crosslinking. *J Membr Sci*. 2016;513:166–76.

Downloaded from academic.oup.com/burnstrauma/article/doi/10.1093/burnst/tkae009/7687763 by guest on 13 October 2026

61. Tasci RO, Kaya MA, Celebi M. Hydrophilicity and flux properties improvement of high performance polysulfone membranes via sulfonation and blending with poly(lactic acid). *High Perform Polym*. 2022;34:1115–30.
62. Gryta M. Surface modification of polypropylene membrane by helium plasma treatment for membrane distillation. *J Membr Sci*. 2021;628:119265.
63. Gryta M. Application of polypropylene membranes hydrophilized by plasma for water desalination by membrane distillation. *Desalination*. 2021;515:115187.
64. Zamel D, Hassanin AH, Ellethy R, Singer G, Abdelmoneim A. Novel bacteria-immobilized cellulose acetate/poly(ethylene oxide) Nanofibrous membrane for wastewater treatment. *Sci Rep*. 2019;9:18994.
65. Bucurescu A, Blaga AC, Estevinho BN, Rocha F. Microencapsulation of curcumin by a spray-drying technique using gum Arabic as encapsulating agent and release studies. *Food Bioprocess Technol*. 2018;11:1795–806.
66. Zhang K, Jiao X, Zhou L, Wang J, Wang C, Qin Y, *et al*. Nanofibrous composite aerogel with multi-bioactive and fluid gating characteristics for promoting diabetic wound healing. *Biomaterials*. 2021;276:121040.
67. Masood N, Ahmed R, Tariq M, Ahmed Z, Masoud MS, Ali I, *et al*. Silver nanoparticle impregnated chitosan-PEG hydrogel enhances wound healing in diabetes induced rabbits. *Int J Pharm*. 2019;559:23–36.
68. Hassan A, Ikram A, Raza A, Saeed S, Zafar Paracha R, Younas Z, *et al*. Therapeutic potential of novel Mastoparan-chitosan Nanoconstructs against clinical MDR Acinetobacter baumannii: in silico, in vitro and in vivo studies. *Int J Nanomedicine*. 2021;Volume 16:3755–73.
69. Seong M, Lee DG. Silver nanoparticles against salmonella enterica serotype Typhimurium: role of inner membrane dysfunction. *Curr Microbiol*. 2017;74:661–70.
70. Ivask A, Elbadawy A, Kaweeteerawat C, Boren D, Fischer H, Ji Z, *et al*. Toxicity mechanisms in Escherichia coli vary for silver nanoparticles and differ from ionic silver. *ACS Nano*. 2014;8:374–86.
71. Qing Y, Cheng L, Li R, Liu G, Zhang Y, Tang X, *et al*. Potential antibacterial mechanism of silver nanoparticles and the optimization of orthopedic implants by advanced modification technologies. *Int J Nanomedicine*. 2018;Volume 13: 3311–27.
72. Nadtoka O, Virych P, Bezugla T, Doroschuk V, Lelyushok S, Pavlenko V, *et al*. Antibacterial hybrid hydrogels loaded with nano silver. *Appl Nanosci*. 2022;12:629–36.
73. Shao J, Wang B, Li J, Jansen JA, Walboomers XF, Yang F. Antibacterial effect and wound healing ability of silver nanoparticles incorporation into chitosan-based nanofibrous membranes. *Mater Sci Eng C Mater Biol Appl*. 2019;98:1053–63.
74. Fazli M, Bjarnsholt T, Kirketerp-Møller K, Jørgensen B, Andersen AS, Krogfelt KA, *et al*. Nonrandom distribution of Pseudomonas aeruginosa and Staphylococcus aureus in chronic wounds. *J Clin Microbiol*. 2009;47:4084–9.
75. Anvarinejad M, Pouladfar G, Japoni A, Bolandparvaz S, Satiary Z, Abbasi P, *et al*. Isolation and antibiotic susceptibility of the microorganisms isolated from diabetic foot infections in Nemazee hospital. *Southern Iran J Pathog*. 2015;2015:328796.
76. Pourmbarak Mahnaie M, Mahmoudi H. Effect of glutathione-stabilized silver nanoparticles on expression of las I and las R of the genes in Pseudomonas aeruginosa strains. *Eur J Med Res*. 2020;25:17.
77. Liu J, Chen Z, Wang J, Li R, Li T, Chang M, *et al*. Encapsulation of curcumin nanoparticles with MMP9-responsive and thermosensitive hydrogel improves diabetic wound healing. *ACS Appl Mater Interfaces*. 2018;10:16315–26.
78. Deng L, Du C, Song P, Chen T, Rui S, Armstrong DG, *et al*. The role of oxidative stress and antioxidants in diabetic wound healing. *Oxidative Med Cell Longev*. 2021;2021:1–11.
79. Xu Z, Han S, Gu Z, Wu J. Advances and impact of antioxidant hydrogel in chronic wound healing. *Adv Healthc Mater*. 2020;9:e1901502.
80. Hamidzadeh K, Christensen SM, Dalby E, Chandrasekaran P, Mosser DM. Macrophages and the recovery from acute and chronic inflammation. *Annu Rev Physiol*. 2017;79:567–92.
81. Kim H, Wang SY, Kwak G, Yang Y, Kwon IC, Kim SH. Exosome-guided phenotypic switch of M1 to M2 macrophages for cutaneous wound healing. *Adv Sci Weinh Baden-Wurtt Ger*. 2019;6:1900513.
82. Krzyszczyk P, Schloss R, Palmer A, Berthiaume F. The role of macrophages in acute and chronic wound healing and interventions to promote pro-wound healing phenotypes. *Front Physiol*. 2018;9:419.
83. Chen Y, Guan M, Ren R, Gao C, Cheng H, Li Y, *et al*. Improved Immunoregulation of ultra-low-dose silver nanoparticle-loaded TiO2 nanotubes via M2 macrophage polarization by regulating GLUT1 and autophagy. *Int J Nanomedicine*. 2020;Volume 15:2011–26.
84. O'Rourke CJ, Munoz-Garrido P, Aguayo EL, Andersen JB. Epigenome dysregulation in cholangiocarcinoma. *Biochim Biophys Acta Mol basis Dis*. 2018;1864:1423–34.
85. Oelschlaegel D, Weiss Sadan T, Salpeter S, Krug S, Blum G, Schmitz W, *et al*. Cathepsin inhibition modulates metabolism and polarization of tumor-associated macrophages. *Cancers*. 2020;12:E2579.
86. Zhao X, Pei D, Yang Y, Xu K, Yu J, Zhang Y, *et al*. Green tea derivative driven smart hydrogels with desired functions for chronic diabetic wound treatment. *Adv Funct Mater*. 2021;31:2009442.
87. Kim SY, Nair MG. Macrophages in wound healing: activation and plasticity. *Immunol Cell Biol*. 2019;97:258–67.
88. Das LM, Binko AM, Traylor ZP, Peng H, Lu KQ. Vitamin D improves sunburns by increasing autophagy in M2 macrophages. *Autophagy*. 2019;15:813–26.

Downloaded from academic.oup.com/burnstrauma/article/doi/10.1093/burnst/tkae009/7687763 by guest on 13 October 2026